

Detecting streaming motions in spiral galaxies

Bachelor Thesis

Author: Jorrit Hagen (s1985892)

Supervisor: Marc Verheijen

Kapteyn Astronomical Institute

June 30, 2013

Abstract

In this research we investigated the streaming motions of the HI gas due to spiral arms in five different spiral galaxies.

To model a velocity field in which streaming motions are excluded, we used the Groningen Image Processing System (GIPSY). The velocity residuals are plotted in a diagram with polar coordinates in which it is easily seen at which radius and azimuthal angle they are located. The same diagram is plotted for the location of the various spiral arms of the galaxies. Streaming motions at positions where spiral arms are located indicate that spiral arms are density waves and carry a gravitational potential.

In this research we did not find a correlation between the amplitude of the observed streaming motions and the amplitude of the HI spiral arm intensities. Such a correlation is also not found between the amplitude of the streaming motions and the amplitude of the r-band spiral arm intensities. We did find streaming motions at radii where HI spirals are visible, but where no structure can be seen anymore in the r-band image, suggesting that the mass of the HI spiral arms is causing these streaming motions.

Contents

1	Introduction	4
2	Used data	4
3	Method	5
3.1	ROTCUR	5
3.2	Initial Estimates	6
3.3	The step-by-step procedure	6
3.4	Weighting Function	7
3.5	SPLINEFIT	8
3.6	The rotation curve	8
3.7	Obtaining the observed residual velocity field	9
3.8	Features of the observed residual velocity field	10
3.9	Turning points	11
3.10	pplot	12
4	Results	13
4.1	NGC2403	15
4.2	NGC3031	18
4.3	NGC3621	25
4.4	NGC5194	28
4.5	NGC6946	33
5	Discussion	36
6	Conclusion	37
7	Future development	37
8	Acknowledgements	38
9	References	38
10	Appendix A: NGC2403	39
10.1	Data	39
10.2	Fitted parameters	41
10.3	Results	43
11	Appendix B: NGC3031 (M81)	45
11.1	Data	45
11.2	Fitted parameters	47
11.3	Results	49
12	Appendix C: NGC3621	51
12.1	Data	51
12.2	Fitted parameters	53
12.3	Results	55

13 Appendix D: NGC5194 (M51)	57
13.1 Data	57
13.2 Fitted parameters	60
13.3 Results	62
14 Appendix E: NGC6946	64
14.1 Data	64
14.2 Fitted parameters	66
14.3 Results	68

1 Introduction

Gas flow motions in spiral galaxies are not perfect circular at a specific radius. Instead of being circular, gas flow velocities slightly vary with azimuthal angle. Gas flows can also have radial (inward or outward) velocity components. Velocities perpendicular to the disk of the galaxies will be ignored. These non-circular motions are caused by the gravitational wells. Spiral arms might induce such wells causing the gas to deviate from circular orbits.

If spiral arms are a standing density wave, then the gas flow of neutral hydrogen should at least be influenced by these spirals. Gas moving away from those spirals will be decelerated and gas moving towards them will be accelerated. These motions are called streaming motions. Far away from those structures the motion of the gas will not be influenced anymore and will move with constant circular speed.

To investigate these streaming motions we first choose a sample of spiral galaxies for which good HI data (21cm) are available, as well as images from other bandpasses to locate the spiral arms. The redshift of the 21cm line of neutral hydrogen will provide us the line-of-sight velocities of the gas. Because low-mass stars contribute the most to the mass of galaxies, especially IR images will be used to trace these stars. Also UV images, which indicate young, high-mass stars, will be used because a relative high number of heavy stars will be born in spiral arms: it makes them good tracers for spirals. After detecting the streaming motions, we will investigate whether there is a correlation between the streaming motions and the amplitudes of the spiral arm intensities from the different bandpasses.

In this research we used the Groningen Image Processing System (GIPSY) to work with the data obtained from different surveys. It is an interactive software system for the reduction and display of astronomical data. We will use GIPSY to model a circular velocity field without streaming motions, which is needed in order to find the streaming motions themselves.

2 Used data

In our research we considered five nearby spiral galaxies. From those five galaxies velocity fields of HI data have already been calculated by The HI Nearby Galaxy Survey (THINGS). We use these data as starting points. It concerns galaxies NGC2403, NGC3031 (M81), NGC3621, NGC5194 (M51a) and NGC6946. For images in the IR bandpass we used data from the Spitzer Survey and the Wide Field Infrared Survey Explorer (WISE) for those galaxies which were not observed by the Spitzer telescope. For images in the UV bandpass we used data from the Galaxy Evolution Explorer (GALEX). For completeness, optical images are taken from the Sloan Digital Sky Survey (SDSS) and the Digitized Sky Survey (DSS) for galaxies that were not observed by Sloan. Because all the galaxies are relatively nearby ($3 < D < 8Mpc$) it is possible to obtain HI maps and velocity fields with high resolution: THINGS has both a high spectral ($\leq 5.2km/s$) and spatial ($6''$) resolution (Walter et al., 2008). We may notice that the galaxies NGC3031 and NGC5194 are tidally interacting with neighboring galaxies, so gas dynamics may be influenced by the companion(s).

Quantity	Galaxy: Units	NGC2403	NGC3031	NGC3621	NGC5194	NGC6946
RA (2000.0)	[hh mm ss.s]	07 36 51.4	09 55 33.2	11 18 16.5	13 29 52.7	20 34 52.3
DEC (2000.0)	[dd mm ss]	+65 36 09	+69 03 55	-32 48 51	+47 11 43	+60 09 14
Distance	[Mpc]	3.51	3.65	6.75	8.00	5.75
V_{sys}	[km/s]	133	-34	730	463	40
PA	[degrees]	122	329	344	162	232
$m_{K_{tot}}$	[mag]	6.191	3.831	6.598	5.496	5.369
m - M	[mag]	27.7	27.8	29.14	29.51	28.76
$M_{K_{tot}}$	[mag]	-21.5	-24.0	-22.5	-24.0	-23.4
V_{rot}	[km/s]	113.6	187.6	140.3	189.3	166.8
Minor axis	[arcmin]	12.3	14.1	7.1	6.9	9.8
Major axis	[arcmin]	21.9	26.9	12.3	11.2	11.5
Ratio		0.562	0.524	0.577	0.616	0.852
Inclination	[degrees]	56.8	59.5	55.7	52.8	32.0

Table 1: Properties of the selected galaxies

3 Method

We used GIPSY to reproject all images to the same pixel-scale and projection system to be able to compare them. This is done because images taken from different surveys are used and every survey uses its own projection. To do this we first loaded the FITS data files into a GIPSY set. We did this by using DSSLOAD for data from DSS or by using RFITS for the other data. After doing this, we were able to reproject the images into the same coordinate system. We used REPROJ to accomplish this. All data were reprojected to the Gnomonic Projection (TAN), simply because most of the data were already projected in this type of projection system. In all data we also changed the rotation angle to 0.0 degrees, so that north points upwards. Because the projection system, pixel scale and the rotation are set equal for all images, we were able to compare them with each other, pixel-by-pixel.

3.1 ROTCUR

We wanted to compare the streaming motions with the position of the spiral arms. As said before we used the velocity field maps of THINGS to fit a rotation curve using the task ROTCUR in GIPSY. This rotation curve models the gas flows in the galaxies as if they are completely circular and constant at a specific distance from the kinematic center. This modeling assumes that no radial motions are present.

3.2 Initial Estimates

In order to improve our rotation curve we fitted the parameters step by step. First we fitted the global properties of the galaxies: the position of the kinematic center and the velocity of the entire system itself. We used information from the NASA/IPAC Extragalactic Database (NED) to estimate values of the central coordinates, the systemic velocity, rotational velocity, position angle and inclination (table 1) which are needed as initial estimates to run ROTCUR. The central coordinates given by NED are coordinates that belong to the optical center. Because the kinematic center may be different from this we have to fit the exact kinematic center. The rotational velocity is initially assumed to be constant at all radii and is computed using the Tully-Fisher Relation in the K band obtained by Verheijen (2001). This relation is given by:

$$M_K = -11.3 \log(2V_{rot}) + 5.12 \quad (1)$$

To find the absolute magnitude of the K band we used the distance modulus and apparent K band magnitude found on the website of the NED. The radial velocities are set to 0.0: we do not want to include them into our modeled velocity field. This is because our streaming motions are defined to be the sum of all motions (including radial velocities) except the pure circular rotational motion of the gas. We initially also assumed the inclination to be constant with radius. We computed the inclination by using the size of the minor and major axis. Then the inclination is simply computed by:

$$\cos(i)^2 = \frac{q^2 - q_0^2}{1 - q_0^2} \quad (2)$$

where q is defined as the observed ratio between the minor and major axis and where q_0 is the intrinsic thickness of the galaxy divided by its diameter (Holmberg, 1958).

We assumed $q_0 = 0.15$, whereas 0.20 is also commonly used.

3.3 The step-by-step procedure

We executed ROTCUR while keeping all the parameters fixed except the parameters we want to fit at that moment. For each fitted quantity we plotted the values against radius to find its global relations. We took a weighted average in regions where small oscillations may be caused by spiral arms, other irregularities or errors by ROTCUR itself, assuming that the errors found by this program are Gaussian (this will give a good approximation of the average). If there were signs of global changes in the plot we modeled the quantity with a linear curve. The kinematic center and velocity of the galaxies are taken constant with radius, which seemed to be correct. The found values in each step are used to replace the estimates in the next step of our fitting procedure.

After finding the kinematic center and the systemic velocity we fitted the position angle (PA), which is defined as the angle at which the line-of-sight velocity at a certain radius is largest, corresponding to the receding side of the galaxy. Because the PA may change with radius, we do not necessarily see this quantity as a constant. The position angle of NGC3031 for example seemed to be constant at radii smaller than 500 arcsec, but at larger radii this angle turned out

Parameter	step 0 (initial estimates)	step 1	step 2	step 3	step 4
Velocity Center	table 1: RA / DEC	FITTED	FIXED	FIXED	FIXED
V_{sys}	table 1	FITTED	FIXED	FIXED	FIXED
PA(r)	table 1	FIXED	FITTED	FIXED	FIXED
Inclination(r)	table 1	FIXED	FIXED	FITTED	FIXED
$V_{rot}(r)$	table 1	FIXED	FIXED	FITTED	FITTED
V_{exp}	[km/s]	0.0	0.0	0.0	0.0
Weighting		UNIFORM	COSINE	COSINE	COSINE

Table 2: Method of determining the rotational velocities

to increase slightly. We now fitted all the parameters except the inclinations and rotational velocities. This is because these are anticorrelated: a larger inclination can induce a lower rotational velocity. This can be seen by noticing that the observed line-of-sight velocity is related to the rotational velocity by the inclination i via (under symmetric assumptions):

$$v_{obs}(r, \theta, i) = v_{sys} + v(r)\sin(i)\cos(\theta) \quad (3)$$

To obtain the best possible fit for the rotational velocity, we first have to fit the inclination, but because the two parameters are related to each other we can not fix the rotational velocity. We also have to fit this parameter at the same time to get reliable results for the inclination. After the inclination is modeled we repeat this procedure, but we will now keep the inclination fixed and improve our just obtained values for the rotational velocity.

3.4 Weighting Function

When fitting the various quantities we used different weighting functions. For the computation of the kinematic center and the systemic velocity we used a uniform weighting function. At every radius we gave all points on the corresponding ellipse of the HI velocity map the same importance: the function **UNIFORM** was used, because velocities on the minor axis also contain information about the systemic velocity. In contrast, we used the cosine weighting function (over the angle from the major axis in the plane of the galaxy) for the determination of the position angles, even though a uniform weighting function would be more obvious. Data along the minor axis contain more information on the position angle than data along the major axis, since the observed velocity field changes the most at the minor axis. The position of the minor axis can therefore be obtained the most accurately. Normal to the minor axis we find the position angle. Around the major axis the observed velocity field does not change a lot, making it less accurate to fit the position angle. On the other hand, strong streaming motions around the minor axis were visible in some of our galaxies, causing wiggles in the observed velocity field at the minor axis. This might result in wrong position angles, so you have to correct for this effect afterwards. We also used a cosine weighting function for the determination of the inclination and rotational velocity, since we are only interested in the circular velocities,

which are best seen at the major axis. At the minor axis only the outward or inward flow of HI can be seen in the observed velocity field: we do not want to correct for these velocities in our model with tangential velocities only. We may note that streaming motions around the major axis can cause peaks and troughs in the fitted rotation curve, since they will have a high weighting. Therefore we modify the fitted rotation curve with a spline.

3.5 SPLINEFIT

At this moment we found the rotation curve for each galaxy. We must note that ROTCUR computed this curve by fitting tilted rings to the observed HI velocity field, which includes all irregularities like streaming motions due to spiral arms. Although we tried to diminish these effects by the step-by-step procedure, the derived velocities still carry some of the effects with them: at radii where spiral arms are prominently present bumps and dips in the rotation curve can be seen, especially when these arms are also located at the major axis where the weighting function is highest. Therefore we assume that these bumps and dips are totally caused by streaming motions induced by the spiral arms, so using the values from ROTCUR will not be correct. Thus, in order to obtain a more smooth rotation curve we fitted a spline to our data points. We used the option SORDER in program SPLINEFIT to subdivide the rotation curve in SORDER-intervals. In each interval the program will calculate the average of the velocities and radii, and will use this point as a control point. Finally it calculates a smooth cubic equation through all the obtained control points. In this procedure the entire original rotation curve is used to get a smoother, more global rotation curve. Note that not all our splines start at (0,0), so the very inner part of the obtained spline is not always useful. We also do not see spiral structures in the inner regions and most of the HI velocity fields are very noisy near the center, so we do not need a good rotation curve at the very inner parts. The cubic spline is used to model our velocity field.

3.6 The rotation curve

To see what the rotation curve will look like, we take a short look at the Newtonian force equation which sets the rotational speeds. In this radial-force equation, the gravitational acceleration equals the centripetal acceleration.

$$\frac{v_{rot}^2(R)}{R} = \frac{GM(< R)}{R^2} \quad (4)$$

$$v_{rot}(R) = \sqrt{\frac{GM(< R)}{R}} \quad (5)$$

Assuming that the mass is uniform distributed (density $\rho = cst$) in a sphere, the rotational velocity will be proportional to R, since $M = \frac{4}{3}\pi\rho R^3$. At large radii, way beyond the 'surface' of this sphere, no more mass will be included and the rotation curve falls with $R^{-0.5}$, since $M(< R)$ will be constant there. Somewhere in between a maximum has to appear.

In reality, spiral galaxies can be seen as disks with densities which drop with

increasing radius. The predicted rotation curve is based on the gravitational potential of a radially exponential distribution of stars in a flat disk. A spiral galaxy can therefore not be seen as a truncate sphere with constant density, but for this purpose it gives a good explanation on the shape of the rotation curve. Observations show that the rotation curves of galaxies are roughly constant or slowly declining at large radii, indicating that there is more mass than we observe: there should be dark matter in the outer regions of the galaxy.

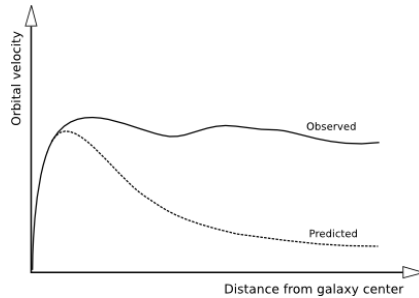


Figure 1: The expected and observed rotation curve of a fictitious galaxy.

3.7 Obtaining the observed residual velocity field

We used the program `VELFI` to model our velocity fields. This program makes a symmetric velocity field: the modeled rotation curve does not depend on azimuthal angle. We must keep in mind that our galaxy might have a velocity field which is not symmetric.

`VELFI` has the same input variables as `ROTCUR` but it now calculates what the observed velocity field would be if all the fitted parameters are correct. The program creates a field by using *equation* [3]. It only needs the fitted parameters (systemic velocity, kinematic center, inclination, position angle and rotation curve). To find the velocity residuals we only have to subtract the model from the observed velocity field.

We used `ELLPROF` to reproject the images from (RA, Dec) sky coordinates to galactic coordinates. With galactic, polar coordinates (θ, r) are meant in the frame where one looks face-on at the galaxy. Obviously r denotes the radius from the galactic center and θ denotes the angle between the position angle and the data point at that radius (counterclockwise). Because the position angle can change with radius, constant θ does not always mean 'in a straight line from the center'.

Since the minor axis is (per definition) smaller than the major axis `ELLPROF` will stretch the data at these positions the most. Relatively few data will be projected into a large range of radii. `ELLPROF` might be less accurate here. Because of this stretching effect, one might overlook features which are clearly seen in the (RA, Dec)-image. It is therefore good to identify streaming motions in the (RA, Dec)-image. On the other hand, `ELLPROF` makes it easy to obtain profiles in both azimuthal and radial direction. We may also note that an increase in azimuthal angle of 1 degree around the minor axis will cause more changes in the observed images than the same increase in azimuthal angle around

the major axis, since all galaxies have a non-negligible inclination and since data along the major axis of a strongly inclined galaxy will be spread out over a large range of azimuthal angles. So, along the minor axis the determination of the radius will be less accurate, but the determination of the azimuthal angle will be more accurate than the same determinations along the major axis. In this report we denote the 'left' and 'right' arm as the arms which are prominently present at angles less than or more than 180 degrees respectively (left and right in the ELLPROF image).

3.8 Features of the observed residual velocity field

The velocity field that results from the HI observations is caused by the flow of the gas. The flow consists of a rotational (or tangential) velocity component, a radial component, and a component perpendicular to the plane of the galaxy (z -axis). This vertical component is neglected since it mostly has values less than 5km/s (van der Kruit & Shostak 1982). Then, in addition to *equation* [3], the line-of-sight velocity becomes:

$$v_{obs}(r, \theta) = v_{sys} + v_{exp}(r, \theta)\sin(i)\sin(\theta) + v_{rot}(r, \theta)\sin(i)\cos(\theta) \quad (6)$$

in which:

v_{sys} is the systemic velocity

v_{exp} is the radial velocity of the HI gas at radius r and azimuthal angle θ

v_{rot} is the tangential velocity of the HI gas at radius r and azimuthal angle θ

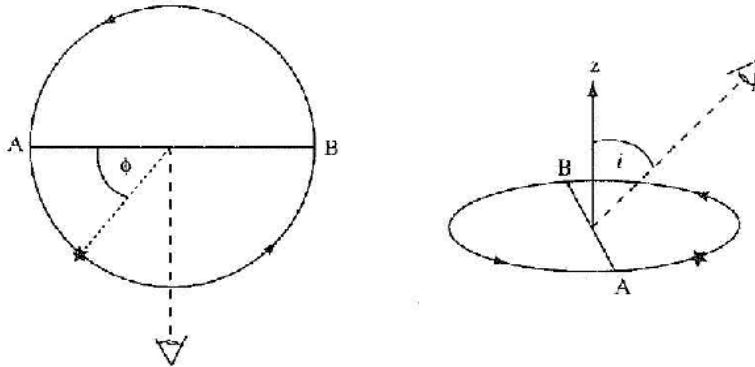


Figure 2: Left: A rotating disk viewed from above. Location B is at the position angle. ϕ is the azimuthal angle. Here it is drawn as angle from A. In this analysis we used the angle θ which is the angle from B ($\theta = \phi + 180^\circ$). Right: The observer's line of sight makes an angle i with the disk's rotation axis z .

Our model only assumes rotational velocities, which also do not depend on θ . Therefore the residual velocity field will consist of the following components:

$$\begin{aligned}
v_{res}(r, \theta) &= v_{obs}(r, \theta) - v_{model}(r, \theta) \\
&= v_{sys} + v_{exp}(r, \theta)\sin(i)\sin(\theta) + v_{rot}(r, \theta)\sin(i)\cos(\theta) \\
&\quad - [v_{sys,model} + v_{rot,model}(r)\sin(i)\cos(\theta)] \\
&= \Delta v_{sys} + v_{exp}(r, \theta)\sin(i)\sin(\theta) + \Delta v_{rot}(r, \theta)\sin(i)\cos(\theta) \\
&= v_{exp}(r, \theta)\sin(i)\sin(\theta) + \Delta v_{rot}(r, \theta)\sin(i)\cos(\theta)
\end{aligned} \tag{7}$$

where $\Delta v_{sys} = v_{sys} - v_{sys,model}$
and $\Delta v_{rot}(r, \theta) = v_{rot}(r, \theta) - v_{rot,model}(r)$
and where we noticed that $\Delta v_{sys} = 0$, since the modeled systemic velocity is (almost) equal to the real systemic velocity.

3.9 Turning points

As a result, turning points will be visible in the residual velocity field. At $\theta = 90^\circ$ or $\theta = 270^\circ$ the term involving $\Delta v_{rot}(r, \theta)$ will switch sign because the cosine does. Also at $\theta = 0^\circ$ or $\theta = 180^\circ$ the term involving $v_{exp}(r, \theta)$ changes sign, because of the dependence on $\sin(\theta)$. So, if the radial velocity is negligible, the observed velocity residuals will change sign at the minor axis. If the tangential velocities are negligible the observed velocity residuals will change sign at the major axis. If neither the radial nor the tangential component of the streaming motion is dominant, you should still see the differences in amplitudes when crossing the concerned axis, but they do not switch sign.

If the spiral pattern in a galaxy is long-lived the spiral arms will move around the galaxy with some angular speed Ω , independent of radius. This means that the rotational speed is low at the central regions and much higher at the outer regions, since $v_{rot} = \Omega \cdot R$. On the other hand, the rotation curve of the gas is flat or slowly declining (after the steep increase in the inner parts of the galaxy). Therefore there should be a point at which the rotational speed of the spiral arms equals the rotational speed of the gas. This is the radius where corotation occurs. Inside corotation the gas catches up with the spiral arm. Outside corotation the arm catches up with the gas. At corotation no gas is entering or leaving the arm and no residual velocities should be visible.

Due to gravitational forces, gas is moving towards the spiral arms with respect to the model. Therefore gas just inside spiral arms will have outward radial velocities and gas just outside the spiral arms inward radial velocities. So, if the spiral arms are gravitational potential wells, you will expect to see different velocity residuals (positive or negative) at different radii (at the same angle θ). At the radius of the potential minimum, which will be near the middle of the spiral arm, the hydrodynamics of the gas flow is complicated, as the gas may experience shocks and compression.

By analogy, the tangential gas velocities will also be influenced by the spiral arms. Relative to the model the gas will move towards the spiral arm. So depending on whether the gas is in front of the arm or behind it, the gas will be decelerated or accelerated respectively.

3.10 pplot

Finally we used the utility `pplot` to make azimuthal (constant radius) and radial (constant angle θ) profiles through the (θ, r) -projected residual velocity fields in order to investigate whether relations between the maxima and/or minima of the streaming motions and the amplitudes of the spiral arms can be found. Option `PROFINT` makes it possible to make a profile over a band with a user-specified width. This will reduce the noise in the profile (higher signal-to-noise), but the accuracy will be less, since data points from other radii/angles will be used as well. In the azimuthal profiles $\Delta\theta = 5$ is taken, to get more smooth profiles. It has the disadvantage that the value at 359° may not be connected to the value at 0° , since averaging over the angles is not possible at the boundaries. The value of $\Delta radnum$ is mentioned at the concerned profile. In the radial profiles `PROFINT` is only used to average over the angle θ . Note that in this report the first value of `PROFINT` denotes $\Delta\theta$, whereas the second value denotes $\Delta radnum$.

4 Results

The results of the step-by-step tilted-ring fitting produce can be seen in tables 3 to 7. In the appendices the graphs of the results are shown. These relations are used to make our models with **VELFI**. The residual velocity fields and the polar projection images can also be found in the appendices.

Fitted Quantity	Galaxy: Units	NGC2403
X center	[grid]	1.72
Y center	[grid]	-0.32
V_{sys}	[km/s]	133.19
PA(r)	[degrees]	PA ($r < 300''$) = 126.0 PA ($300'' < r < 1250''$) = 126.0 - 0.00421($r - 300$)
Inclination(r)	[degrees]	$i(r < 200'')$ = 58.0 $i(200'' < r < 800'')$ = 58.0 + 0.011667($r - 200$) $i(800'' < r < 1250'')$ = 65.0

Table 3: The fitted relations for NGC2403

Fitted Quantity	Galaxy: Units	NGC3031
X center	[grid]	0.16
Y center	[grid]	-0.32
V_{sys}	[km/s]	-36.38
PA(r)	[degrees]	PA ($r < 500''$) = 329.82 PA ($500'' < r < 900''$) = 329.82 + 0.0117($r - 500$) PA ($900'' < r < 1100''$) = 334.5
Inclination(r)	[degrees]	$i(r < 650'')$ = 59.39 $i(650'' < r < 1100'')$ = 59.39 + 0.0258($r - 650$)

Table 4: The fitted relations for NGC3031

Galaxy:		NGC3621
Fitted Quantity	Units	
X center	[grid]	-3.97
Y center	[grid]	-3.78
V_{sys}	[km/s]	728.90
PA(r)	[degrees]	PA ($r < 400''$) = 345.09 PA ($400'' < r < 630''$) = $345.09 + 0.085696(r - 400)$ PA ($630'' < r < 830''$) = $364.8 + 0.016(r - 630)$
Inclination(r)	[degrees]	$i(r < 300'')$ = 65.02 $i(300'' < r < 600'')$ = $65.02 - 0.022(r - 300)$ $i(600'' < r < 830'')$ = 58.4

Table 5: The fitted relations for NGC3621

Galaxy:		NGC5194
Fitted Quantity	Units	
X center	[grid]	-1.67
Y center	[grid]	0.16
V_{sys}	[km/s]	459.37
PA(r)	[degrees]	172.39
Inclination(r)	[degrees]	41.52

Table 6: The fitted relations for NGC5194

Galaxy:		NGC6946
Fitted Quantity	Units	
X center	[grid]	-0.38
Y center	[grid]	-2.85
V_{sys}	[km/s]	42.53
PA(r)	[degrees]	PA ($r < 200''$) = 236.0 PA ($200'' < r < 550''$) = $236.0 + 0.03143(r - 200)$ PA ($550'' < r < 750''$) = $247.0 - 0.06807(r - 550)$ PA ($750'' < r < 1000''$) = 233.39
Inclination(r)	[degrees]	33.51

Table 7: The fitted relations for NGC6946

4.1 NGC2403

NGC2403 does not have clear spiral arms. The spiral structure consists of many small spiral arms: HI can be seen over the entire galaxy. The produced model is in good agreement with the observed velocity field, but it is smoothed now. Unfortunately, the residual velocity field does not show clear streaming motions, probably because there are no big gravitational potential wells because of the weak spiral structure.

A better look at the residual velocity field shows that there are small streaming motions. In figure 3 azimuthal profiles are shown at radius number 115. Although we do not see a distinct HI spiral arm, we still see an increase in HI intensity around 260 degrees. On either side of this maximum streaming motions occur.

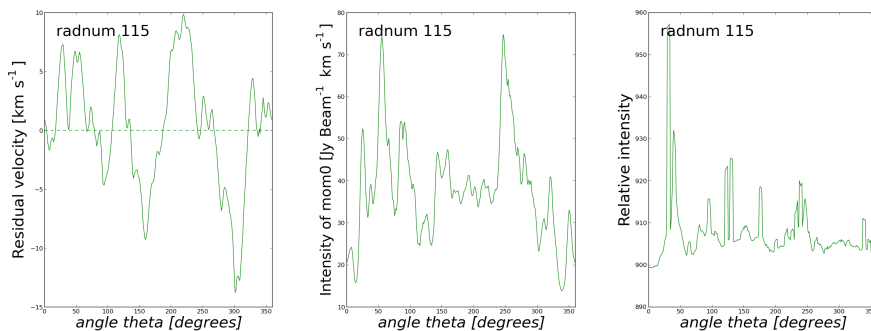


Figure 3: Azimuthal profiles taken from the observed residual velocity field (left), the HI intensity map (center) and the r-band intensity map (right) at radius number 115 (5.8 kpc). Around $\theta = 260^\circ$ the HI intensity is maximum. At the same azimuthal angle no maximum can be seen in the r-band profile. Instead, three bright point sources are visible. A maximum ($\theta = 240^\circ$) in the observed residual velocity profile changes to a minimum ($\theta = 300^\circ$). These streaming motions are induced by the high HI intensity. [PROFINT=5 30]

Also two radial profiles are taken, at $\theta = 38^\circ$ and $\theta = 100^\circ$ (figure 4). At these azimuthal angles small streaming motions are visible. At $\theta = 38^\circ$ and $r = 200$ arcsec the HI intensity is maximum and the residual velocities change rapidly from negative to positive values. At $\theta = 100^\circ$ two weaker maxima in HI intensity are visible around $r = 210$ arcsec and $r = 380$ arcsec. Both maxima seem to influence the HI gas velocity, since the small streaming motions ($< 10\text{ km/s}$) vary from minus to plus 10 km/s in the range from 180 to 540 arcsec. In between the spiral arms, at 300 arcsec, the streaming motions are constant and almost negligible.

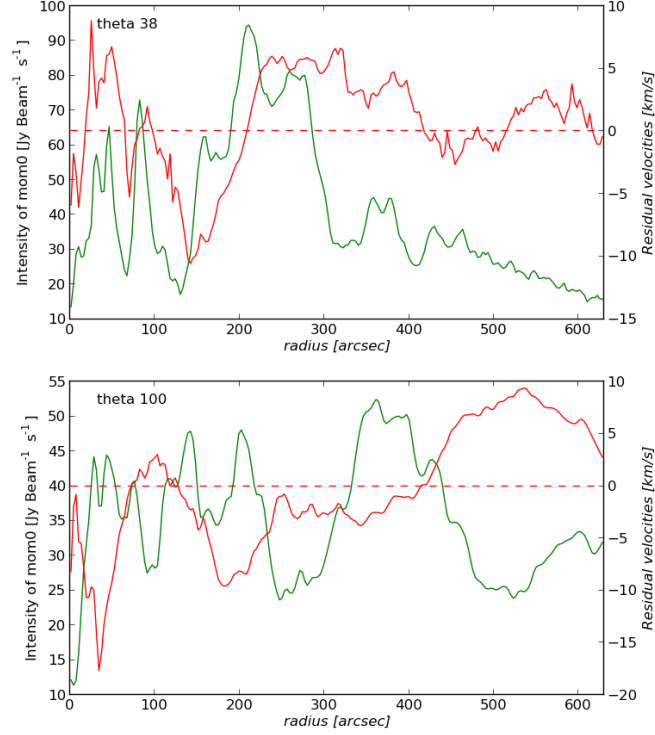


Figure 4: Radial profiles taken from the observed residual velocity field (red, right y-axis) and the HI intensity (green, left y-axis) at 38 and 100 degree in azimuthal angle. Note that the limits of the x-axis correspond with radius numbers 1 (lower limit) to 210 (upper limit). [PROFINT=20 0]

We will now compare our model with the observed HI velocities along the minor and major axis. In figure 5 it can be seen that the observed HI velocities correspond to the modeled velocities, except at the minor axis at 270 degrees, where the model has velocities which are 5 km/s higher than the observed HI velocities. In the last column the profiles on the minor axis are averaged. The same is done with the profiles on the major axis. The averaged velocities are correct for the western minor axis and the northern major axis.

Although the model seems to be pretty good, no strong streaming motions can be seen. Few weak streaming motions can be seen, but only in small parts of the galaxy. Therefore we are not able to investigate a possibly correlation between HI spiral arm amplitudes and amplitudes in the observed residual velocities in NGC2403.

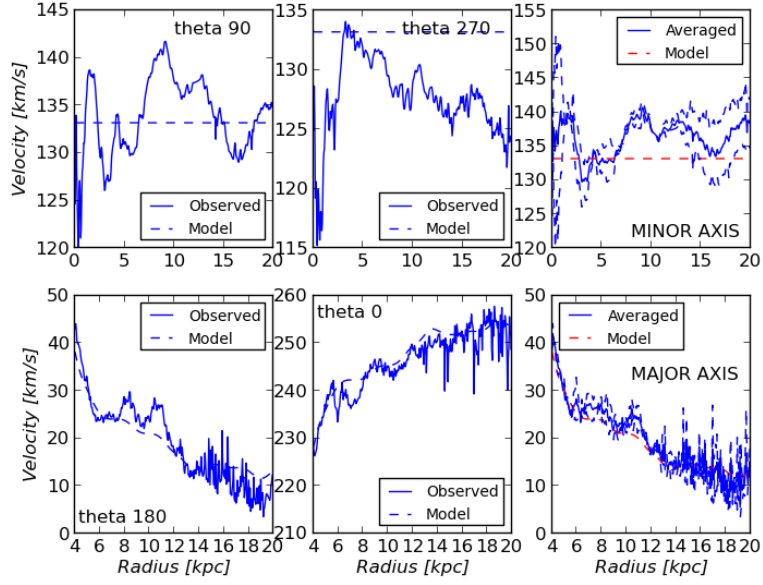


Figure 5: Radial profiles taken from the observed HI velocity field along the minor axis (upper row) and the major axis (lower row). The dashed lines show the velocity curved used in our model of NGC2403. The last column contains the averaged velocities, that correspond to the western minor axis ($\theta = 90^\circ$) and the major northern axis $\theta = 180^\circ$. [PROFINT=25 0]

4.2 NGC3031

NGC3031 has very bright spiral arms, visible in the r-band and over a much larger region in HI. Here the model is also in accordance with the observed velocity field. In this galaxy clear streaming motions are visible around 110 and 280 degrees in azimuthal angle. Several turning points are visible. The reversal of the sign of the velocity residuals after crossing the spiral arms can be seen most prominently. At an angle of 90 degrees this also happens. This can be explained by the prediction that the radial velocities are negligible here compared to the tangential velocities, but this is not likely. The tangential velocities need to be very high to produce these results. We will discuss this later on. At lower azimuthal angles (around 80 degrees) the velocity residuals are approaching on the inside and receding on the outside of the spiral arms, at higher angles (around 110 degrees) this is vice versa. This is in agreement with *equation* [7]. This switch does not appear around $\theta \approx 270^\circ$.

Visser (1980) found a corotation radius at 11.3 kpc, Rots and Shane (1975) found a corotation radius at 10.3 kpc. Roughly around radius number 205 (615 arcsec) we see that the velocity residuals are very weak at azimuthal angles below 200 degrees. This can be seen in the polar projection of the residual velocity field (see appendix B). This may indicate the corotation radius, which is then located at 10.8 kpc under our assumptions.

In figures 6 and 7 azimuthal profiles at five different radii are shown. Figure 6 shows the observed residual velocity as a function of azimuthal angle. Figure 7 shows profiles of the spiral arm intensities in HI and the r-band. Note that the location of the peaks are separated by roughly 180° , as expected. In table 8 the maxima and minima in the residual velocity profiles that are located around the spiral structures can be found. In tables 9 and 10 the intensity amplitudes of the corresponding HI spiral arms and r-band spiral arms can be found.

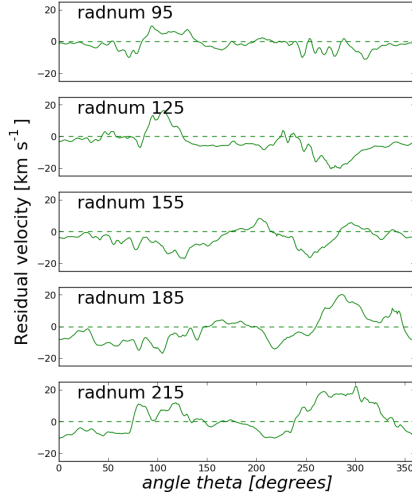


Figure 6: Azimuthal profiles taken from the observed residual velocity field. The minima and maxima of the residual velocity field move along with the peaks in intensity of the HI spiral arms, as seen in the next figure. [PROFINT=5 30]

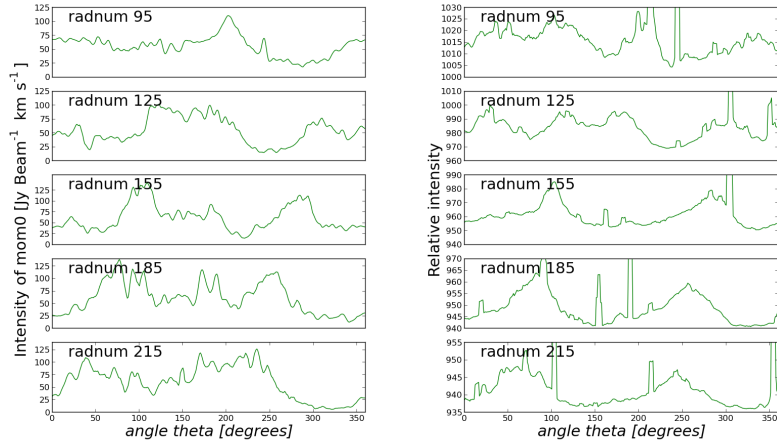


Figure 7: Left: Azimuthal profiles taken from the HI map. Right: The same profiles, but now taken from the r-band field. At radius number 125 ($6.6kpc$) the left spiral arm is almost flat: the peak gets a big shift to higher angles. The minima and maxima of the residual velocity field move along with the peaks in intensity of the HI and r-band spiral arms. [PROFINT=5 30]

NGC3031 Radnum	Residual field kpc	angle	minimum	angle	maximum
Left Arm					
95	5.0	–	–	94	10.1
125	6.6	–	–	107	16.9
155	8.2	127	-16.7	–	–
185	9.8	105	-16.6	–	–
215	11.4	–	–	119	12.1
Right Arm					
95	5.0	310	-11.0	–	–
125	6.6	276	-20.1	–	–
155	8.2	254	-16.2	296	6.0
185	9.8	219	-14.0	287	20.5
215	11.4	219	-10.2	301	22.6

Table 8: Properties of the observed residual velocity profiles.

NGC3031 Radnum	HI integrated map kpc	angle	maximum
Left Arm			
95	5.0	203	110.7
125	6.6	123	101.8
155	8.2	110	142.6
185	9.8	78	138.7
215	11.4	39	109.9
Right Arm			
95	5.0	350	67.6
125	6.6	311	77.1
155	8.2	285	113.8
185	9.8	258	113.7
215	11.4	236	127.3

Table 9: Properties of the HI profiles.

NGC3031	r-band image	ref	angle	maximum	amplitude
Radnum	kpc				
Left Arm					
95	5.0	1004.5	206	1023.6	19.1
125	6.6	969.3	118	996.0	26.7
155	8.2	950.8	104	985.2	34.4
185	9.8	940.9	82	964.0	23.1
215	11.4	936.0	61	948.1	12.1
Right Arm					
95	5.0	1004.5	326	1019.1	14.6
125	6.6	969.3	290	985.8	16.5
155**	8.2	950.8	276	973	22
185	9.8	940.9	257	959.6	18.7
215**	11.4	936.0	242	946	10

Table 10: Properties of the r-band profiles. The column named 'ref' shows the values of the minima in every profile. We calculated the amplitude by subtracting this background intensity from the maximum intensity of the spiral arm. ** position and amplitude are estimated. (point sources obscure the maximum)

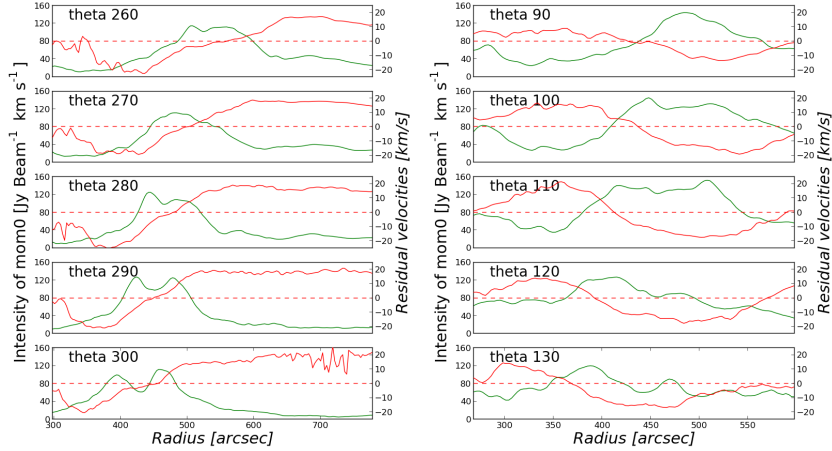


Figure 8: Left: Radial profiles of the left spiral arm taken from the residual (red) velocity field and HI (green) map. Right: The same profiles, but now from the right spiral arm. In these vertical profiles we see that the residual velocities switch sign where the HI intensity is highest. At the minor axis we can estimate the value of the radial velocities. Assuming this velocity to be constant along a spiral arm, we can also estimate the tangential velocities of the streaming motions. [PROFINT=10 0]

Now we will estimate the actual, in-plane velocities of the streaming motions near the minor axis, using the radial profiles of figure 8. At 270° a difference in residual velocities of 39 km/s can be obtained from the profiles. Using *equation* [7] with $i = 59.39^\circ$, this equals 44.3 km/s difference in radial velocities between the gas outside and the gas inside the spiral arm (roughly -22 and +22 km/s respectively). Assuming that this difference is constant within 10° of the minor axis, the difference in tangential velocities can be estimated. At 260° and 280° we find a difference of -15.2 and 44.7 km/s in tangential velocities. Averaging the absolute(!) values gives an estimation of 30 km/s (roughly -15 (outside) and +15 km/s (inside)). At this minor axis the radial velocities are therefore 50% stronger than the tangential residual velocities. The total residual speed is roughly $\sqrt{22^2 + 15^2} \approx 27$ km/s. So motions perpendicular to the disks with velocities smaller than 5 km/s can indeed be neglected.

At the other minor axis (90°) we find a much lower radial velocity at the position of the spiral arm: the difference in velocity between the gas outside and inside the arm is 26.2 km/s (roughly -13 and +13 km/s respectively). Assuming this value to be constant we obtain tangential velocities to be equal ± 45 km/s, where we only used the profile at 100 degrees. This confirms that at this minor axis the tangential velocities are indeed higher than the radial velocities, but they are not sufficiently high to explain the '90°-turning point'.

We must note that these calculations of the tangential velocities are not very accurate, since the observed residual velocities due to the tangential velocities are very weak near the minor axis. These observed 'extra' velocities might as well be caused by a small change in radial velocities: we won't assign any significance to it. The average of the tangential velocity around 270° is calculated by averaging the absolute values. Note that the sign changes from minus (-15.2) to plus (44.7), which is not plausible.

We compared the THINGS data with the data from the Westerbork Synthesis Radio Telescope (WSRT) which Visser (1980) used. In figure 9, the observed HI velocities are plotted along minor and major axis. The last column shows the plots with the averaged observed velocities (solid blue line). These velocities are correct for the eastern minor axis $\theta = 90^\circ$ and southern major axis $\theta = 180^\circ$. The dashed lines represent the data from either side of the center to show the differences. The dashed red line represents the model we used to obtain the residual velocity field. The plots are in agreement with those of Visser, but our figure is based on data with higher resolution, so the model Visser made can be improved. Note that we assume a distance of 3.65 Mpc and a systemic velocity of -36.4 km/s, whereas Visser used a distance of 3.25 Mpc and a systemic velocity of -40 km/s. This is the reason why our data points are shifted to the right and why the averaged curves have a slightly different amplitude in comparison with Visser. In the plots it is easily seen whether the model fits the observed velocities or not or at which radius streaming motions appear along the minor and major axis.

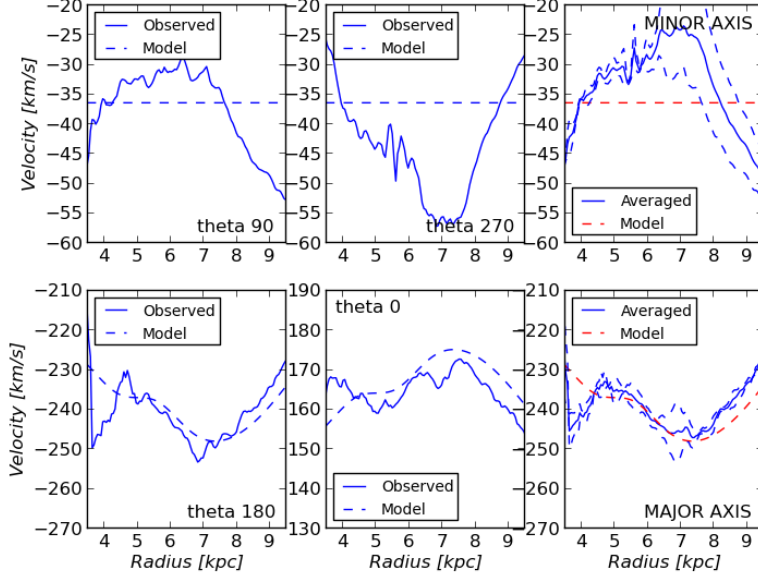


Figure 9: Similar plots like Visser did. The residual velocities are small along the major axis. [PROFINT=25 0]

Since NGC3031 has very bright and distinct spiral arms, the arms are also prominent over a large range in radius, especially the HI spiral arms. Therefore we are able to plot the amplitudes of the HI and r-band spiral arm intensities as a function of the observed residual velocity amplitudes at the same radius, as seen in figure 10. We assumed the HI amplitudes to be equal to the maximum intensity in the azimuthal profiles, although we subtracted a reference intensity (ref) from the maximum r-band intensity. The corresponding coordinates can be seen in tables 8 to 10.

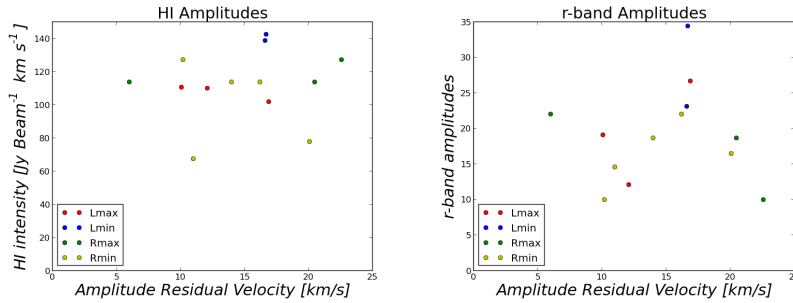


Figure 10: Left: Results from the HI spiral arms. Right: Results from the r-band spiral arms. On the y-axis the amplitudes of respectively the HI and r-band spiral arm intensities, at the different radii, are shown as a function of the corresponding minimum or maximum observed residual velocities (x-axis).

There does not seem to be any relation between the amplitude of the spiral arm intensities and the amplitude of the observed residual velocity field on the basis of the r-band image. One might even draw a curve which predicts a higher residual velocity as the amplitude of the r-band spiral arm intensities decreases. Of course this would be nonphysical since streaming motions are expected to be stronger with increasing strength of the spiral arm.

The results of the HI amplitudes compared with the amplitudes of the corresponding residual velocities also do not show a correlation.

Note again that we assumed that the HI inter-arm intensity equals zero, although we estimated the r-band inter-arm intensity (background) to be equal to the smallest value in every profile.

Also note that the residual velocities depend on the angle θ , for which no correction could have been made, since we could not obtain the physical components of the tangential and radial velocities in this research. A more advanced simulation is needed to fit the observed velocities to the theoretical formula, using the simulation. This procedure was done by Shetty et al. (2007). We also did not correct for the inclination, which would result in higher residual velocities by a factor of $1/\sin(59.39) \approx 1.16$, if we did.

4.3 NGC3621

NGC3621 has no bright spiral arms in the optical image. HI spiral arms can be seen in the very outer region of the galaxy, at radii ($r > 450$ arcsec) where our modeled velocity field is not reliable anymore (see appendix C). Therefore we can not compare the intensity amplitudes of the spiral arms with the amplitudes in the streaming motions.

In figures 11 and 12 azimuthal profiles of the residual velocities, the HI intensities and the r-band intensities are shown. No r-band spiral arms are visible in the profiles. Around $\theta = 330$ arcsec, at radius numbers 60 and 75, negative observed residual velocities are visible, but there is no clear spiral pattern visible in the HI profile. The HI spiral structure does show up at radius number 95, at the same azimuthal angle. At this radius, however no streaming motions are visible anymore. The amplitudes of the two minima in the residual profiles and the maximum in the HI intensity profile are shown in table 11.

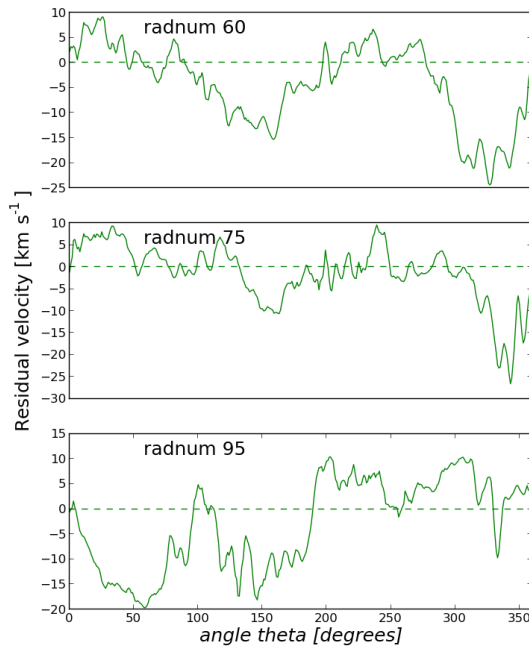


Figure 11: Azimuthal profiles taken from the observed residual velocity field at the radii where streaming motions are visible. The used radius numbers are 60 (300 arcsec), 75 (375 arcsec) and 95 (475 arcsec), which correspond to 9.8, 12.3 and 15.5 kpc. [PROFINT=5 10]

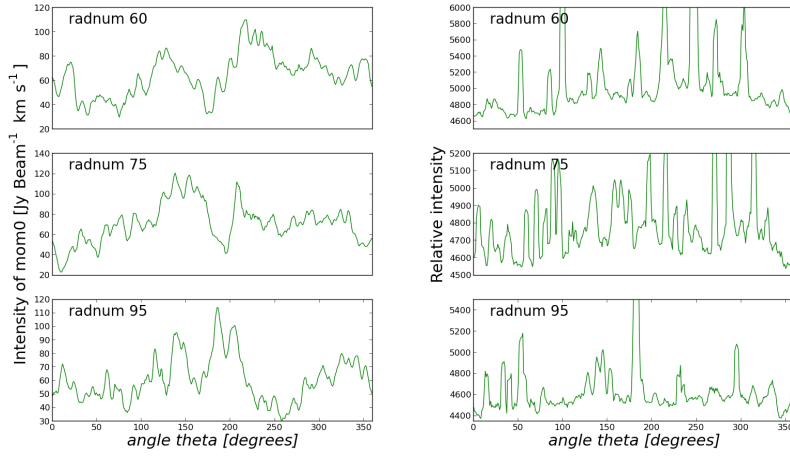


Figure 12: Left: Azimuthal profiles taken from the HI map. Right: The same profiles, but now taken from the r-band field. At radius number 95 (475 arcsec) no peak in the HI profile can be seen at the azimuthal angles where residual velocity minima are observed. This confirms that the model is not good anymore at this radius. Unfortunately also no peaks in the HI profile can be seen around $\theta = 300^\circ$ at radius numbers 60 and 75. At the same azimuthal angle and radius number 95 the HI spiral arm is visible in the profile. [PROFINT=5 10]

NGC3621	Residual field	angle	minimum
Radnum	kpc		
Right Arm			
60	9.8	328	-24.4
75	12.3	344	-26.6
NGC3621	HI integrated map		
Radnum	kpc	angle	maximum
Right Arm			
95	15.5	326	80.3

Table 11: Properties of the observed residual velocity profiles and the HI profiles.

Again we compare our modeled velocities along the minor and major axes with the observed HI velocities. In figure 13 it can be seen that the observed HI velocities along the minor and major axes start to differ from each other at roughly 17 kpc (roughly 500 arcsec). Therefore it is harder to model a good velocity field, since each side of the galaxy contains different information. The observed HI velocity field is not symmetric anymore at these radii. This is in agreement with our statement that the model is less reliable at $r > 450$ arcsec. We can explain this by taking a look at the observed HI velocity field. The eastern side of the galaxy contains large streaming motions (see the iso-velocity contours of the observed velocity field in appendix C). The western side is not changed by streaming motions. ROTCUR fitted the parameters using both sides of the galaxy, resulting in a velocity field that does not match the unperturbed western side of the galaxy. For the model it had been better to use this part of the galaxy only.

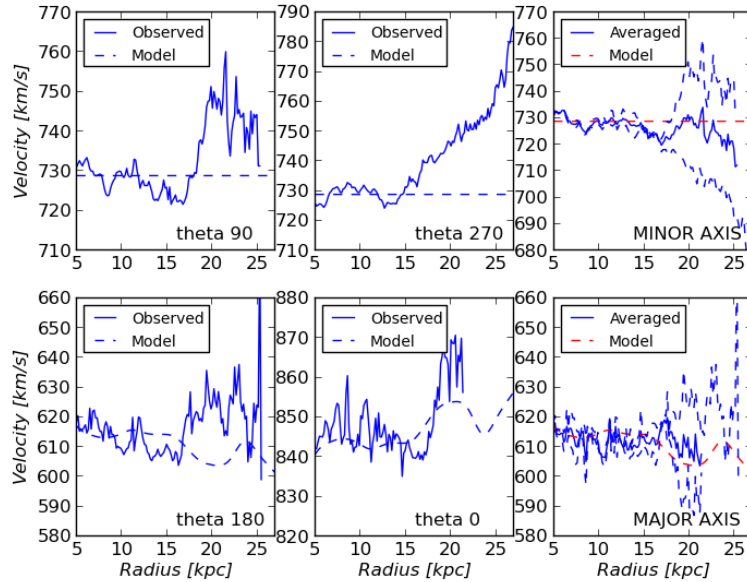


Figure 13: Similar plots like Visser did. [PROFINT=25 0]

4.4 NGC5194

NGC5194 has bright spiral arms, but it is interacting with its companion. The observed velocity field is not symmetric at $r > 250$ arcsec. The model is less good at these radii. In the observed residual velocity field only a strong positive or negative velocity is found per arm (not both). The left arm only has a clear negative part, the right arm only a positive part. The reverse parts can probably be seen at larger radii, outside this image.

In figures 14 and 15, we show the azimuthal profiles of the residual velocities, the HI intensities and the r-band intensities at the radius numbers where streaming motions are visible. In tables 12, 13 and 14, the obtained amplitudes with corresponding azimuthal angles are shown. If no value is given in the table, then no clear amplitude is visible in the corresponding profile at the corresponding spiral arm.

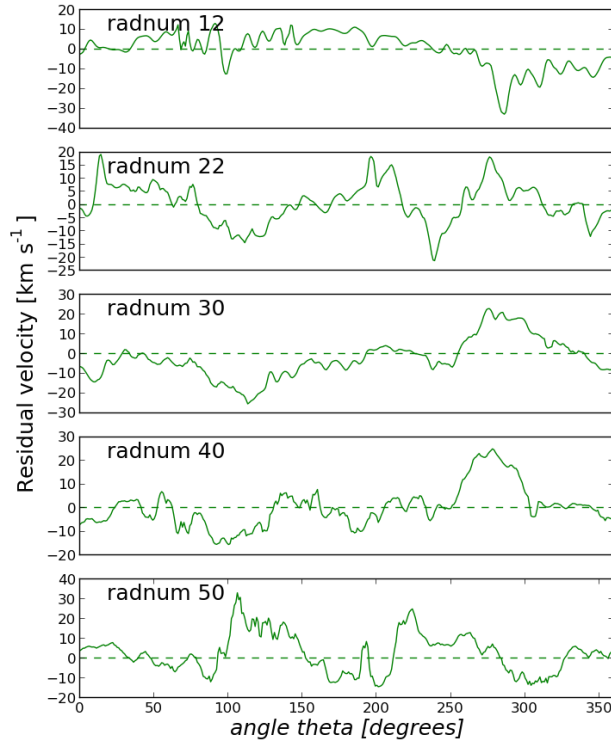


Figure 14: Azimuthal profiles taken from the observed residual velocity field. It is hard to see which of the minima and maxima of the residual velocity field correspond to the peaks in intensity of the HI spiral arms. Comparing the profiles with the galactic coordinate image gives a better view. See the tables for the results. [PROFINT=5 10 (at radnum 12: 5 5)]

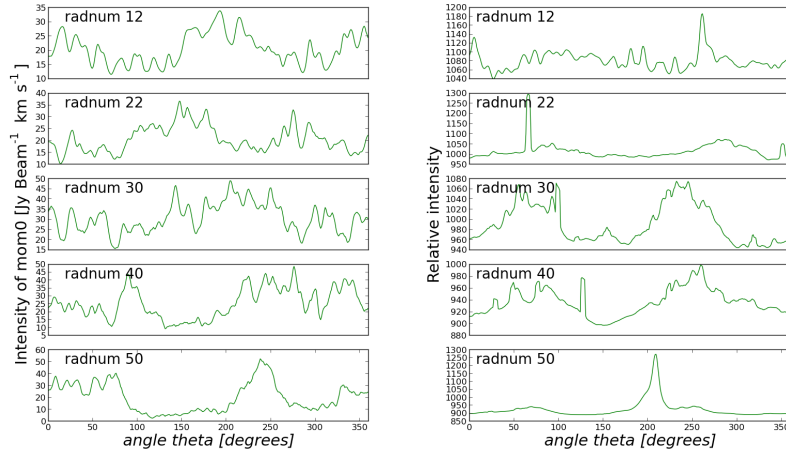


Figure 15: Left: Azimuthal profiles taken from the HI field. Right: The same profiles, but now taken from the r-band field. At radius number 30 ($5.7kpc$) the left spiral arm is almost flat. It has a broad peak, with smaller peaks on top of it. The first peak is chosen to use after comparing the HI field with the residual velocity field. The spiral arms in the r-band are much more clear, but we must note that these profiles also include point sources. [PROFINT=5 10 (at radnum 12: 5 5)]

NGC5194	Residual field				
Radnum	kpc	angle	minimum	angle	maximum
Left Arm					
12	2.2	—	—	—	—
22	4.1	112	-14.3	—	—
30	5.7	114	-25.2	—	—
40	7.6	101	-15.3	—	—
50	9.5	—	—	—	—
Right Arm					
12	2.2	—	—	—	—
22	4.1	240	-21.1	277	18.3
30	5.7	—	—	277	22.9
40	7.6	—	—	279	25.0
50	9.5	—	—	225	25.1

Table 12: Properties of the observed residual velocity profiles.

NGC5194	HI integrated map		
Radnum	kpc	angle	maximum
Left Arm			
12	2.2	194	33.9
22	4.1	118	27.2
30	5.7	144	46.8
40	7.6	90	43.8
50	9.5	77	40.4
Right Arm			
12	2.2	–	–
22	4.1	276	33.0
30	5.7	–	–
40	7.6	277	48.8
50	9.5	239	52.6

Table 13: Properties of the HI profiles.

NGC5194	r-band image				
Radnum	kpc	ref	angle	maximum	amplitude
Left Arm					
12	2.2	–	–	–	–
22	4.1	973.3	93	1054.7	81.2
30**	5.7	944.9	75	1030	85
40	7.6	897.5	87	964.8	67.3
50	9.5	891.3	70	942.7	51.4
Right Arm					
12	2.2	–	–	–	–
22	4.1	973.3	288	1074.0	100.8
30	5.7	944.9	233	1075.2	130.3
40	7.6	897.5	260	998.7	101.2
50	9.5	891.3	253	945.5	54.2

Table 14: Properties of the r-band profiles. ** The value of the peak around 75° is estimated to be 1030. A bright point source obscures this peak. Other examples of bright point sources are found at radnumber 22, angle 70° , and at radnumber 50, angle 210° .

In figure 16 we compared our modeled observed velocities along the minor and major axes with the observed HI velocities. We can conclude that our model is good at the both axes. We see that streaming motions are only visible at the minor axis, which can also be seen in the observed residual velocity field with (θ, r) -coordinates.

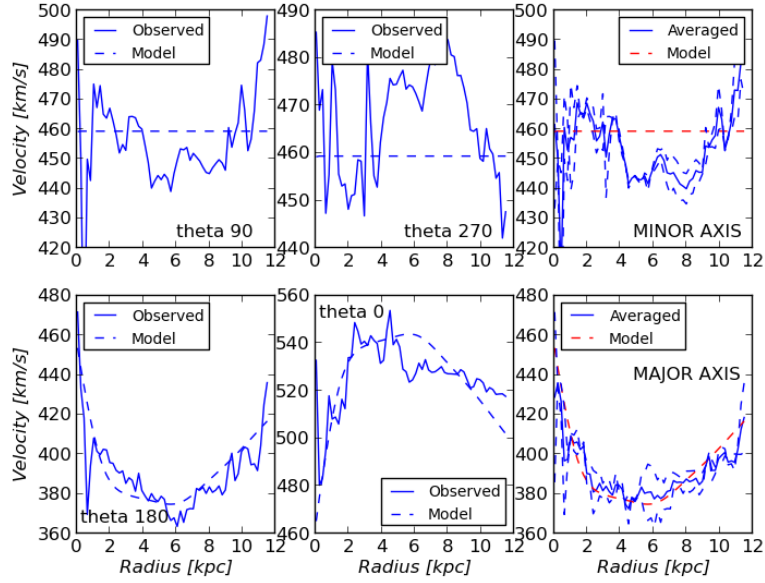


Figure 16: Similar plots like Visser did. The residual velocities are again small along the major axis. Along the major axis the observed HI velocities are in accordance with the velocities in our model. The averaged profiles are correct for the western minor axis and the northern major axis. [PROFINT=25 0]

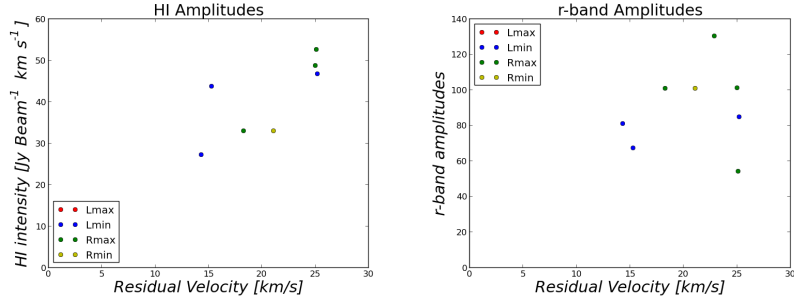


Figure 17: Left: Results from the HI spiral arms. Right: Results from the r-band spiral arms. On the y-axis the amplitudes of respectively the HI and r-band spiral arm intensities, at the different radii, are shown as a function of the corresponding minimum or maximum observed residual velocities (x-axis).

As seen in figure 17, there does not seem to be a correlation in HI or r-band image between the spiral intensity amplitude and the amplitude in the observed residual velocity field. Nevertheless a weak correlation in the plot with HI amplitudes might be visible: $I_{HI} \approx 2V_{res}$, but it is just as likely to conclude that no relation can be found. Note that the residual velocities also depend on the angle θ , for which no correction could have been made. We also did not correct for the inclination, which would result in higher residual velocities by a factor of $1/\sin(41.52) \approx 1.51$, if we did.

4.5 NGC6946

NGC6946 has visible spiral arms, but it is difficult to identify a small region where the arms are located, since these arms consist of many subarms. The spiral arms are broad and the HI is distributed over the entire galaxy. The observed velocity field is not symmetric at $r > 700$ arcsec. Therefore our model is less good at these radii. In the observed residual velocity field only positive residual velocities are obtained in the outer regions at 100° azimuthal angle. This is caused by the HI spiral structure, but we must also note that the model is less reliable here (see appendix E).

In figures 18 and 19 azimuthal profiles of the residual velocities, the HI intensities and the r-band intensities are shown at radii where the observed velocity field seems to show (small) streaming motions. A r-band spiral arm is only visible in the profile with radius number 45 (225 arcsec). The HI spiral arms extend to much larger radii and are much better visible. Assuming that our model is good up to radius number 135 (675 arcsec), we can obtain the HI spiral arm amplitudes and the corresponding residual velocity amplitudes. These values are shown in table 15.

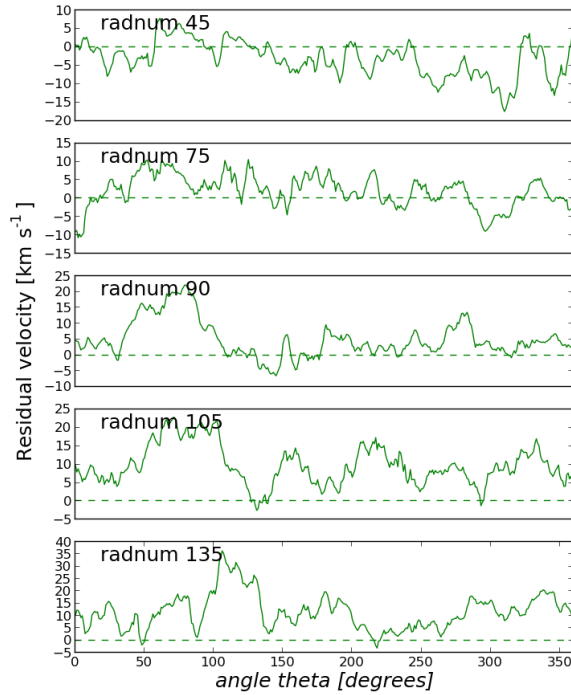


Figure 18: Azimuthal profiles taken from the observed residual velocity field. Clear streaming motions are only visible at radius numbers 90, 105 and 135. [PROFINT=5 10]

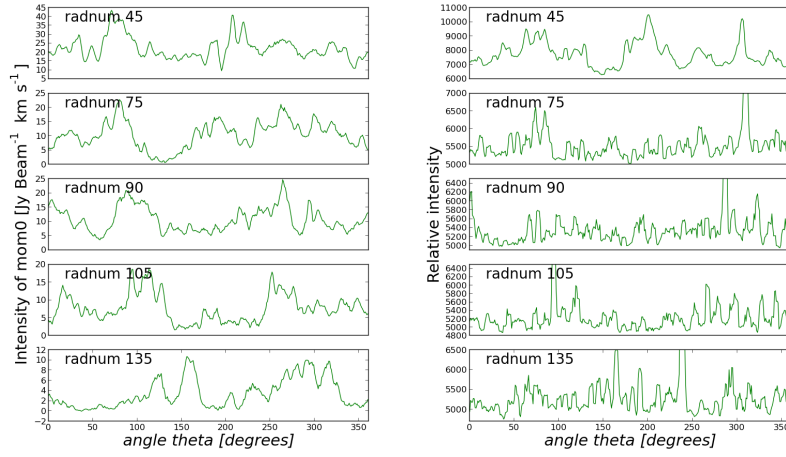


Figure 19: Left: Azimuthal profiles taken from the HI map. Right: The same profiles, but now taken from the r-band field. The maxima of the residual velocity field seem to move along with the peaks in intensity of the left HI spiral arm, suggesting that HI might induce streaming motions (since no spiral arm is visible in the r-band profiles). [PROFINT=5 10]

NGC6946 Residual field		angle	maximum
Radnum	kpc		
Left Arm			
90	12.4	80	22.2
105	14.5	72	22.8
135	18.6	107	36.4
NGC6946 HI integrated map			
Radnum	kpc	angle	maximum
Left Arm			
90	12.4	88	20.9
105	14.5	114	18.6
135	18.6	157	10.7

Table 15: Properties of the observed residual velocity profiles and the HI profiles.

As seen in figure 20 it is not possible to conclude whether there is a correlation between the spiral intensity amplitudes and the amplitudes in the observed residual velocity field. The three points that are shown do not support the hypothesis that the observed streaming motions are stronger at higher spiral arm intensities. Note that the residual velocities also depend on the angle θ , for which no correction could have been made. We also did not correct for the inclination, which would result in higher residual velocities by a factor of $1/\sin(33.5) \approx 1.81$, if we did.

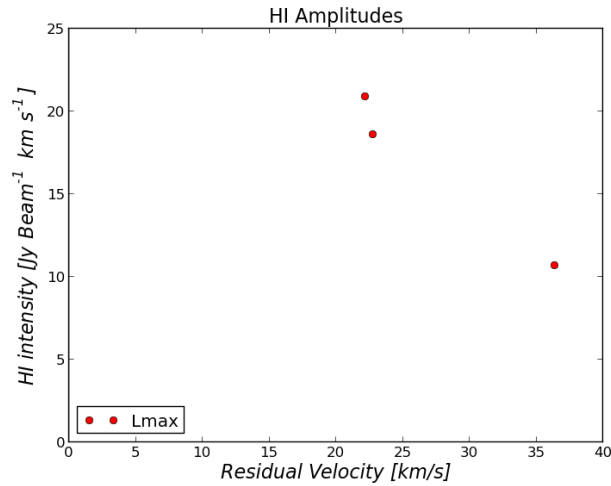


Figure 20: Plot of the HI spiral arm amplitudes as a function of amplitude in residual velocity. We were only able to use three data points under the assumption that our model is correct. No correlation can be obtained.

In figure 21 we compared our modeled observed velocities along the minor and major axes with the observed HI velocities. The averaged profiles are correct for the western minor axis and the northern major axis. We can conclude that the observed velocity profiles at the minor axis start to differ from each other at roughly 11 kpc (radius number 80). At the major axis this also happens, but at a larger radius (17kpc, which corresponds to radius number 120). The model is therefore less reliable at these radii.

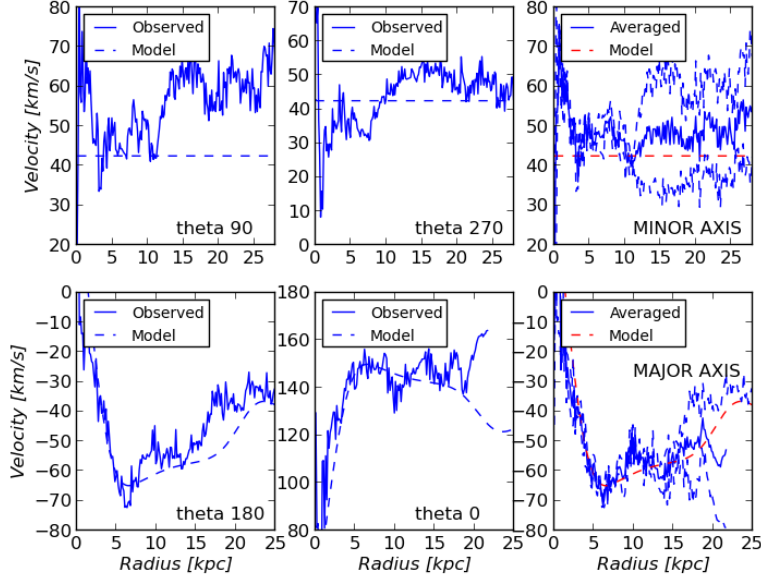


Figure 21: Similar plots like Visser did. [PROFINT=25 0]

5 Discussion

We must note that the errors given by the GYPSY task ROTCUR are computed with the assumption that the individual data points of the input image all have the same error, because we did not specify those uncertainties. This is definitely not true. The error bars in the plots only give an estimation of the real errors. We may further note that we produced horizontal profiles in order to compare our results to the ones of Shetty et al. (2007), even though vertical profiles sometimes show stronger amplitudes in the residual velocity field. Unfortunately we were not able to obtain the actual, in-plane velocities, so we could not compare our results with the results of that research. Taking horizontal profiles gave us the possibility to investigate whether the streaming motions decrease with decreasing amplitude of the HI spiral arms or with decreasing amplitude of the r-band (stellar) spiral arms or both, since the HI spiral arms extend to much larger radii than the stellar spiral arms.

Not all of the profiles were continuous at the boundaries as stated before. It had been better to execute ELLPROF from negative azimuthal angles to azimuthal angles larger than 360. Then pplot with option PROFINT would work properly around 0 and 359 degrees in azimuthal angle.

We also may note that the residual velocities do not give a understanding of the physical, radial and tangential, velocities. In order to estimate those real values we need to compare the observed velocity field with the velocities obtained from a model of the galaxies, the way Shetty et al. (2007) did. In addition, we plotted the maximum in intensity of the spiral arms, although we also might have chosen to compute the total intensity (by integrating the profile). We also

could have computed gradients of the streaming motions and spiral arm intensities. We estimated the r-band amplitude by subtracting the minimum of the azimuthal profile from the arm intensity, although we did not do this for the HI spiral arms. All kind of different approaches are possible.

Our models are completely symmetric, whereas the observed galaxies aren't. For each galaxy we made the assumption that it was symmetric in the inner regions as discussed. This had the disadvantage that large parts of the galaxy were not useful anymore. In some of the galaxies strong streaming motions were visible at the edge of the model. It was not always obvious whether these motions were only caused by the spiral arms. Streaming motions could also be induced when the symmetric assumption in the galaxy might not be true anymore.

After all, we decided only to compare the streaming motions with the HI and r-band intensities. We did not use the IR (Spitzer/WISE) band, since their intensity maps seem not to be that different from the r-band maps. We didn't also use the UV (Galex) band. These maps are more like the HI intensity maps and the 'UV spiral arms' are extended to larger radii than the r-band arms, but to smaller radii than the HI spiral arms.

6 Conclusion

In this research we detected the streaming motions of 5 nearby spiral galaxies. Detecting streaming motions can be done by subtracting a modeled velocity field from the observed velocity field, obtained from HI data. In order to make the model the kinematic center, systemic velocity, position angle, inclination and rotational velocity of the galaxy have to be fitted.

Only galaxies with very clear spiral arms have distinct maxima and/or minima in their observed residual velocity field. No correlation has been found between the amplitudes of the observed residual velocities and the amplitudes of the spiral arm intensities in the HI integrated map and the r-band image. We did show that streaming motions occur at radii where no r-band spiral arms can be seen anymore. Therefore, streaming motions seem to be caused by the HI mass in the spiral arms. The influence of the mass of the stars (r-band image) in the spiral arms on the streaming motions is not clear.

7 Future development

We might conclude that it is hardly possible to classify spiral galaxies based on their observed streaming motions. Very clear streaming motions seem to indicate clear spiral arms. But more galaxies have to be studied to make a statement.

As said before, it would be better to evaluate physical residual velocities rather than observed residual velocities. The observed maximum in the residual velocity field might have a different location than the maximum of the physical velocity. Fitting the observed velocities to modeled velocities or other assumptions would be necessary. At the minor and major axes it is possible to calculate the physical radial and tangential velocities respectively, since the other component is not observable there. Assuming these quantities to be constant at a

small width in azimuthal angle around these axes makes it possible to measure the other velocity component. But then one might wonder whether the remaining weak residual velocities are caused by that other velocity component or that they are a consequence of the assumption. In this research we did not find reliable results using this method, but other approaches might be more successful. It is interesting to investigate whether there is an evident relation between the amplitudes and/or gradients of the streaming motions and the amplitudes and/or gradients in intensity of the spiral structure. Then more galaxies have to be studied. The same can be done with the physical tangential and radial velocities. This can be done in different bands in order to understand whether streaming motions are dominantly caused by the mass of HI gas (HI) or by the mass of the stars: old stars (r-band) and/or young hot stars (u-band).

8 Acknowledgements

First of all I would like to thank my supervisor Marc Verheijen for spending lots of time with me to help me to finish this small research. You learned me to work with GIPSY and helped me to understand the physical problems I encountered. I also would like to thank the computer group, especially Martin who fixed problems in GIPSY tasks and helped me to plot contours and coordinate grids in the produced images. I thank Wim for his advice just to wait (... almost an hour) when the computer was rebooting by mistake. I almost thought something bad was going on. I also thank him for immediately getting a new screen when my previous one decided to stop working properly. Eite made it possible to use the Virgo01 machine at the time my own machine, Whipple, had used its entire data directory. I did not have to use Virgo01, but if I had to, I could continue my project. Also many thanks to the students of room 134 who answered questions about some silly programming errors.

9 References

- Holmberg, E.B.: 1958, *Med. Lunds Astron. Obs.* **II**, No. 136
Rots, A.H., Shane, W.W.: 1975, *Astron. Astrophys.* **45**, 25
Shetty, R., Vogel, S.N., Ostriker, E.C., Teuben P.J.: 2007, *Astrophys. J.* **665**, 1138
van der Kruit, P.C., Shostak, G.S.: 1982 *Astron. Astrophys.* **105**, 351
Verheijen, M.A.W.: 2001, *Astrophys. J.* **563**, 694
Visser, H.C.D.: 1980, *Astron. Astrophys.* **88**, 149 & 159
Walter, F., Brinks, E., de Blok, W.J.G., Bigiel, F. Kennicutt, Jr., R.C., Thornley, M.D., Leroy, A.: 2008, *Astrophys. J.* **136**, 2563

DATA obtained from THINGS, Spitzer Survey, WISE, GALEX, SDSS, DSS
Initial estimates from NASA/IPAC NED

Used book for background information:

Sparke, L.S., Gallagher, J.S., III.: 2007, *Galaxies in the Universe: An introduction*, (second edition), Cambridge: Cambridge University Press

10 Appendix A: NGC2403

10.1 Data

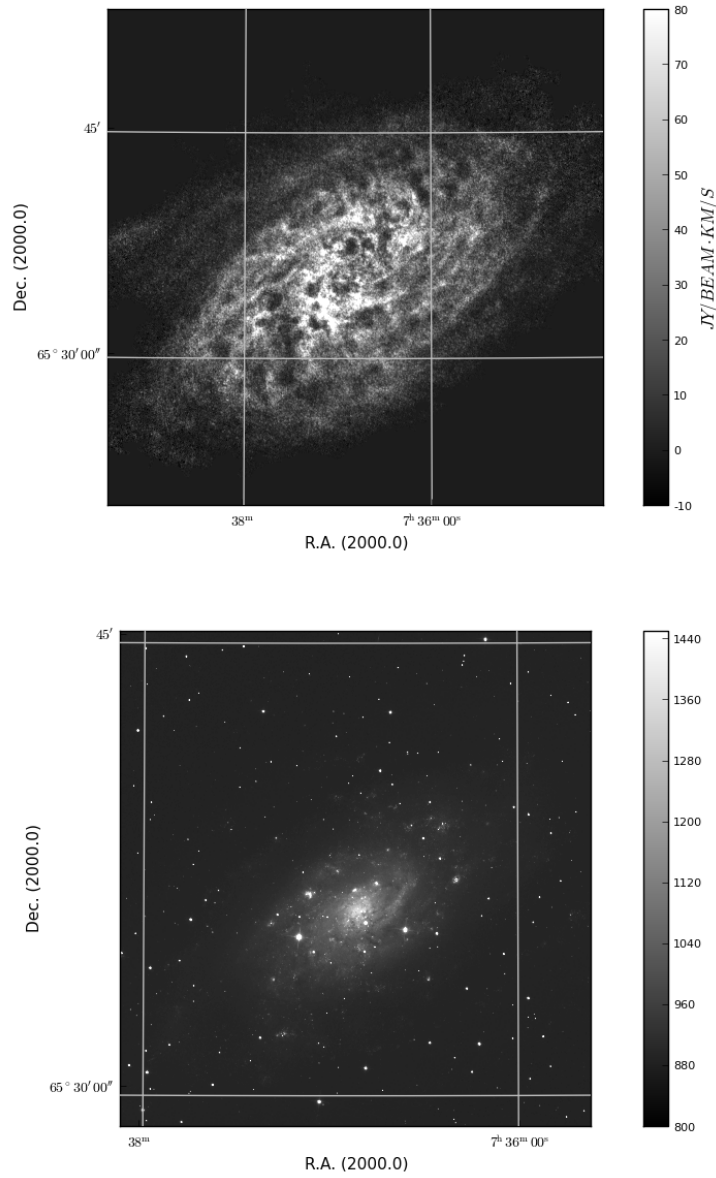


Figure 22: Upper image: Integrated HI map (THINGS). There are lots of 'HI clouds' visible, but there are no clear spiral arms. Lower image: Optical image (r-band) taken from SDSS (note the scale difference). [$15 \text{ arcmin} = 15 \text{ kpc}$]

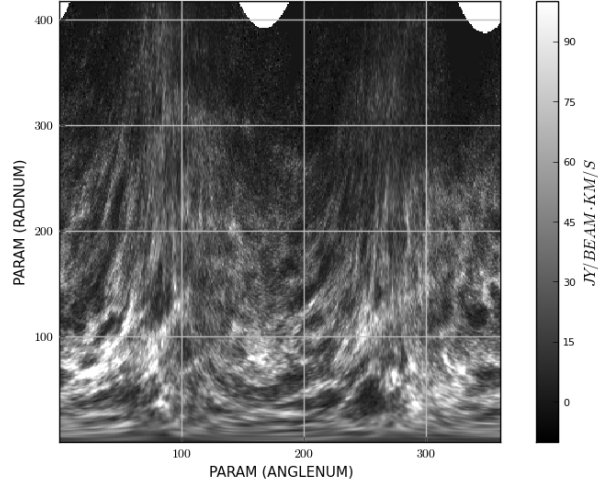


Figure 23: The same integrated HI map, but now in galactic coordinates. On the x-axis the angle θ is shown. It is defined to be angle from the position angle taken in anti-clockwise direction. On the y-axis the radius number is shown. In this image an increase of 1 radnum means an increase of 3 arcseconds in radius. Although it is difficult to see spiral arms in the integrated HI map small bands can surely be seen, but they are not prominent.

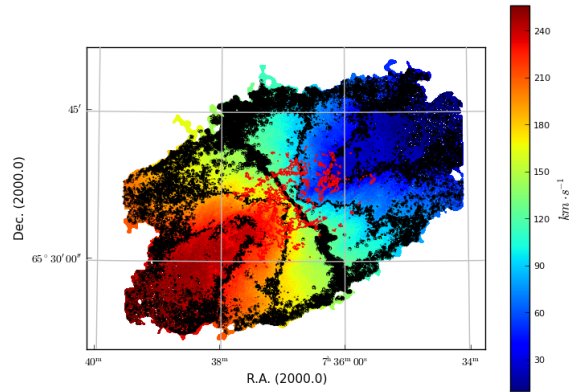


Figure 24: Observed HI velocity field with iso-velocity contours (black) spaced by 50 km/s around the systemic velocity at 133 km/s. A contour of the HI integrated map is also drawn in red indicating relative high amounts of HI.

10.2 Fitted parameters

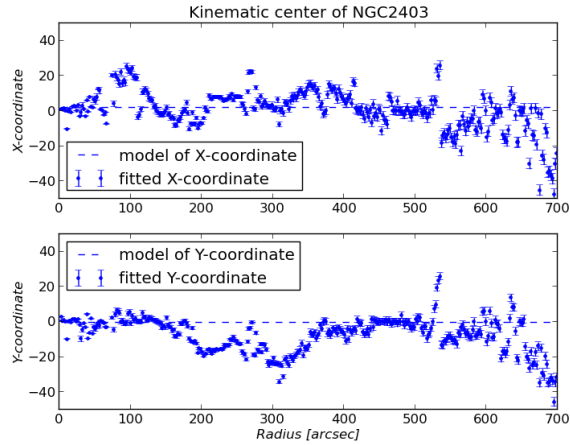


Figure 25: ROTCUR fits the dotted values. The dashed lines show the used values for the kinematic center (model) in the next fitting steps. The fitting is done over the inner part of the galaxy (max. radius is 700 arcsec). The kinematic center is assumed to be constant over the entire galaxy.

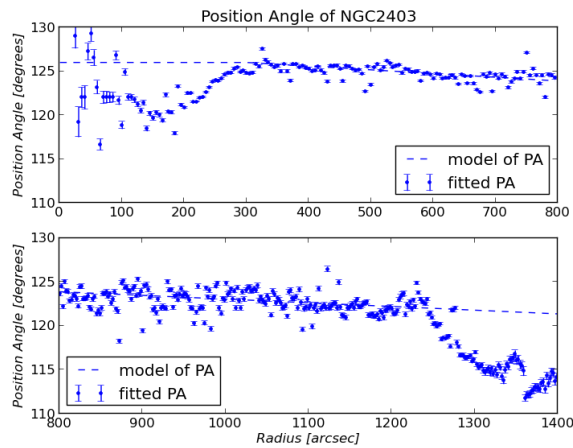


Figure 26: ROTCUR fits the dotted values. The dashed line shows the used curve (model) in the next fitting steps. Note that the model does not match the fitted values anymore at radii smaller than 300 and larger than 1250 arcsec. In the center we assume the model has a more smooth character. At large radii the number of data points decreases very quickly. Ellipses are not fully occupied by data points anymore: we take out those results.

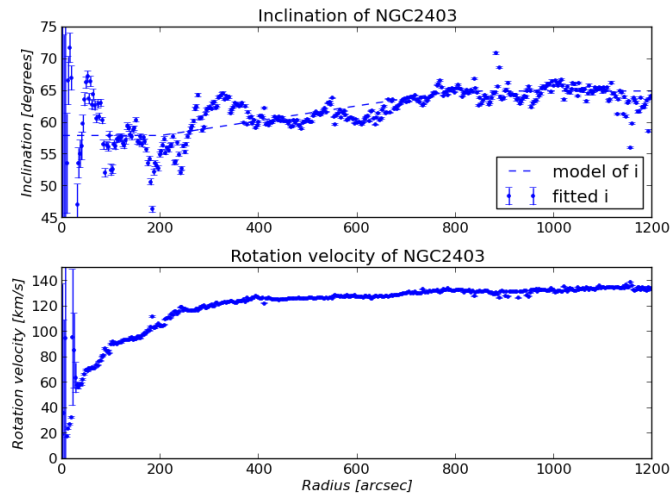


Figure 27: ROTCUR fits the dotted values. The dashed line shows the used curve (model) in the next fitting step. At the very inner part (< 200 arcsec) the inclination is assumed to be constant.

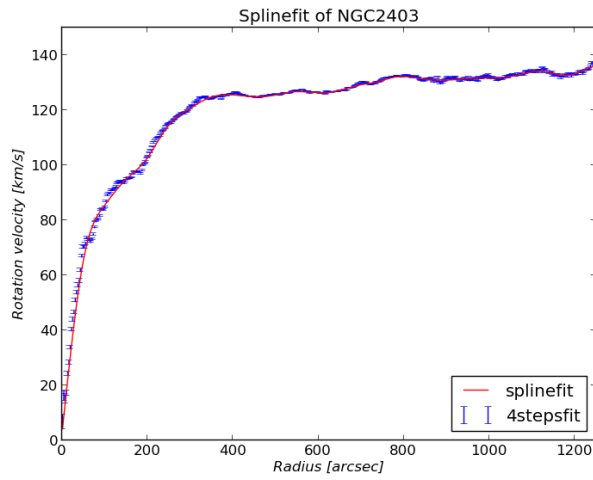


Figure 28: ROTCUR fits the blue values determined while letting the inclination constant at the inner regions. The red line shows the used curve in our modeled velocity field. We did not change the rotation curve a lot, but is continuous now.

10.3 Results

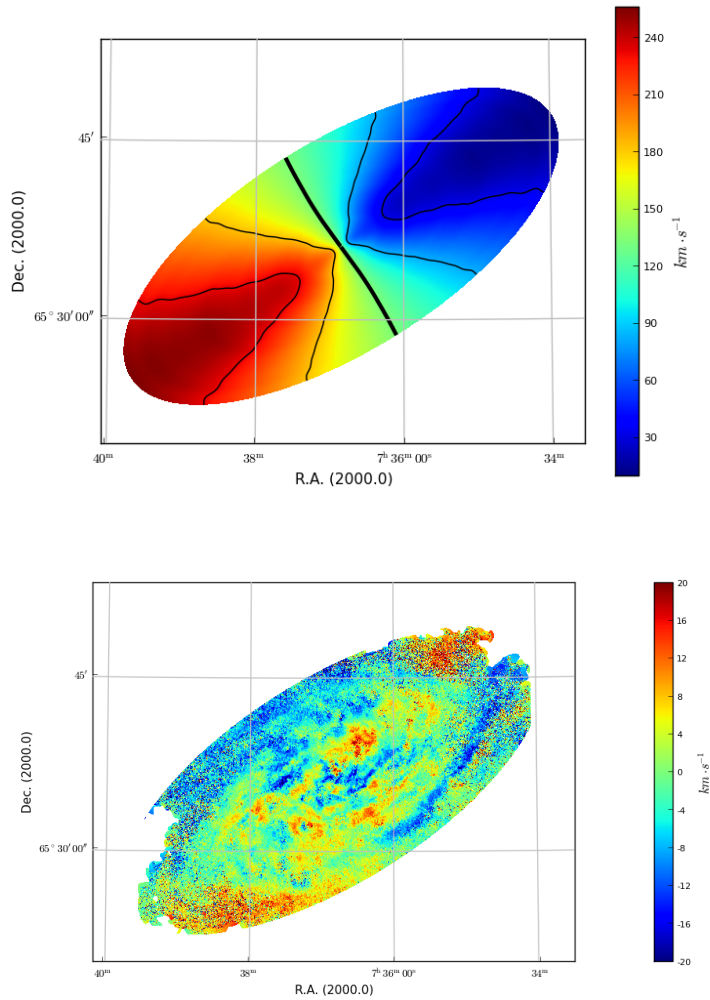


Figure 29: Upper image: Shown is the modeled velocity field created by the program VELFI. All the modeled parameters from the step-by-step procedure are used. Contours are shown spaced by 50 km/s around the systemic velocity of 133 km/s. Lower image: Shown is the observed residual velocity field obtained by subtraction the modeled velocity field from the observed one. There are no clear streaming motions visible. Nevertheless you can see small ones around the minor axis.

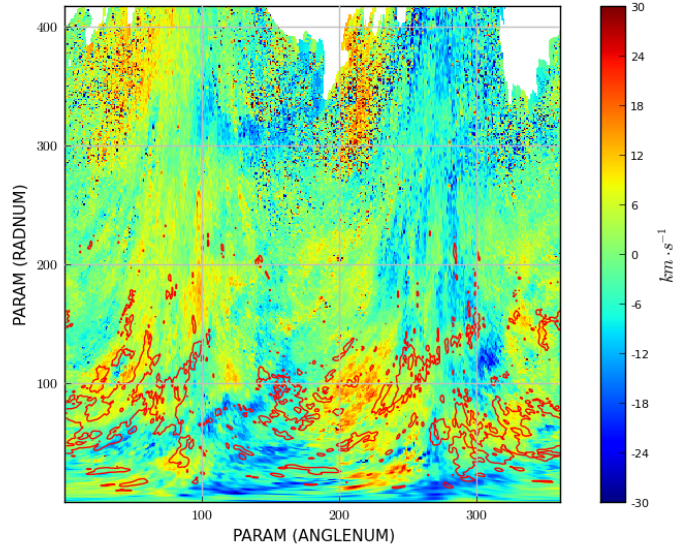


Figure 30: The same observed residual velocity field but now in the galactic coordinates. A contour of the HI image is also shown. Around angle number 120 and radius number 80 a small relation between spiral structure and residual velocities can be seen.

11 Appendix B: NGC3031 (M81)

11.1 Data

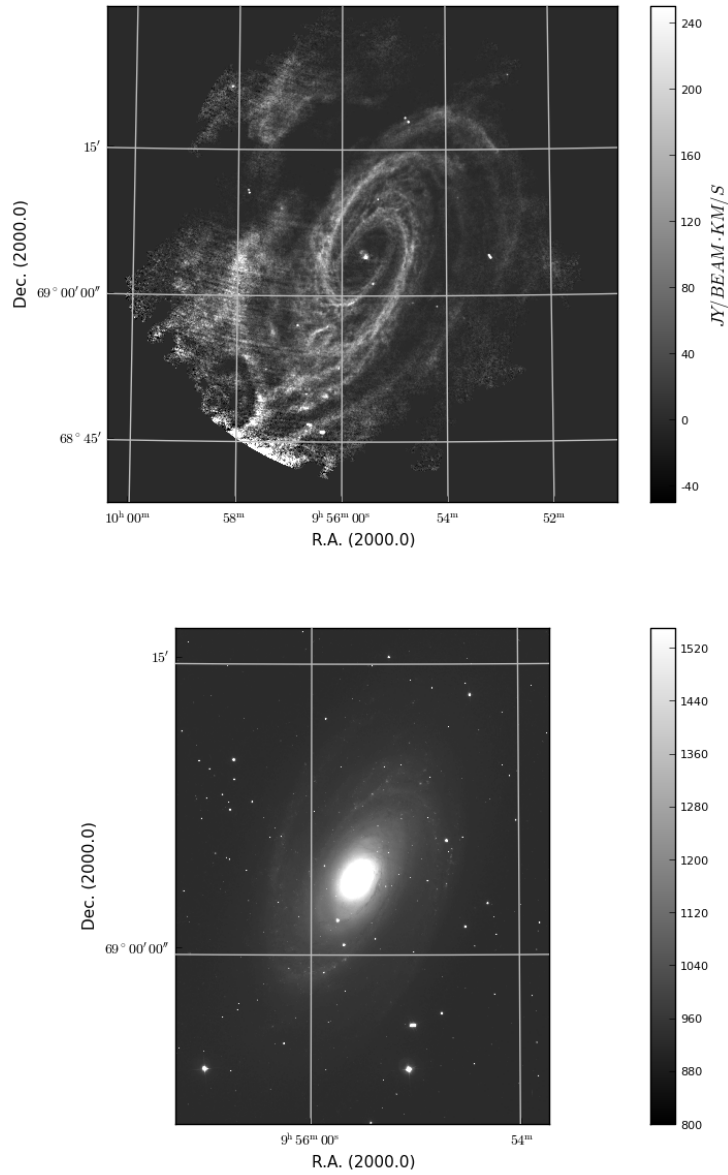


Figure 31: Upper image: Integrated HI map (THINGS). Lower image: Optical image (r-band) taken from SDSS. The structure of the spiral arms are also visible in this image, but less clear and only in the inner regions. [$15\text{arcmin} = 16\text{kpc}$]

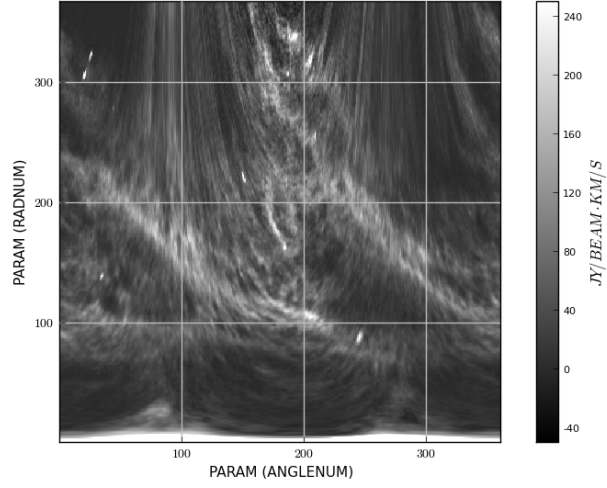


Figure 32: The same integrated HI map, but now in galactic coordinates. On the x-axis the angle θ is shown. It is defined to be angle from the position angle taken in anti-clockwise direction. On the y-axis the radius number is shown. In this image an increase of 1 radnum means an increase of 3 arcseconds in radius.

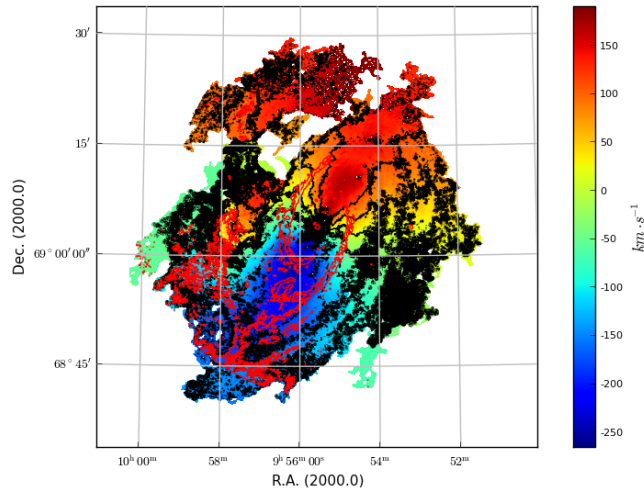


Figure 33: Observed HI velocity field with iso-velocity contours (black) spaced by 50 km/s around the systemic velocity at -36 km/s. A contour of the HI spiral arms is also drawn in red.

11.2 Fitted parameters

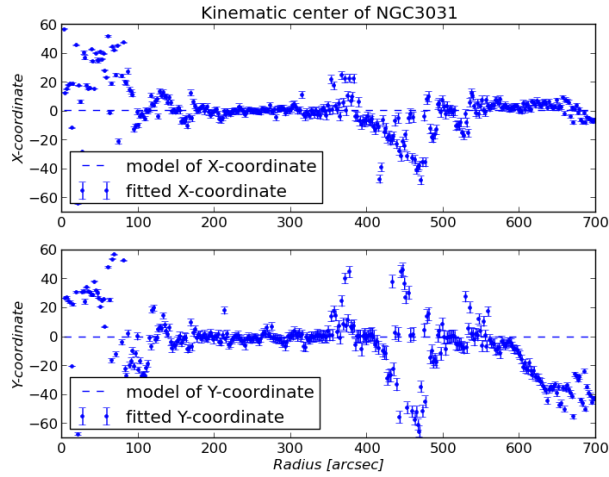


Figure 34: ROTCUR fits the dotted values. Dashed lines show the used values for the kinematic center (model) in the next fitting steps.

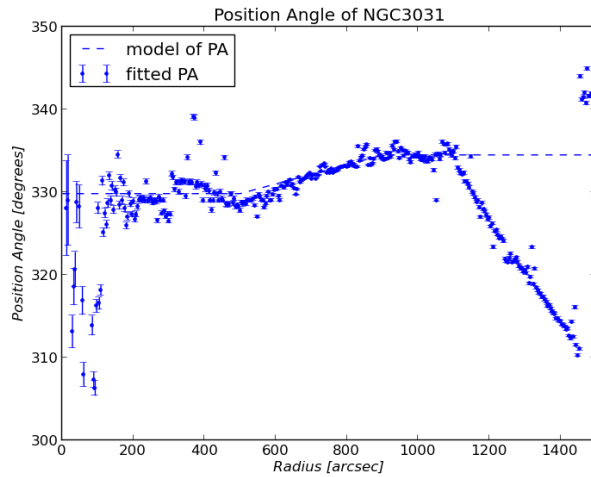


Figure 35: ROTCUR fits the dotted values. The dashed line shows the used curve (model) in the next fitting steps. Note that the model does not match the fitted values anymore at radii larger than 1100 arcsec. This is not important since we will not use these values: at those radii from the kinematic center, the interactions with other member of the M81-group starts to play a great role in the dynamics of the gas flow.

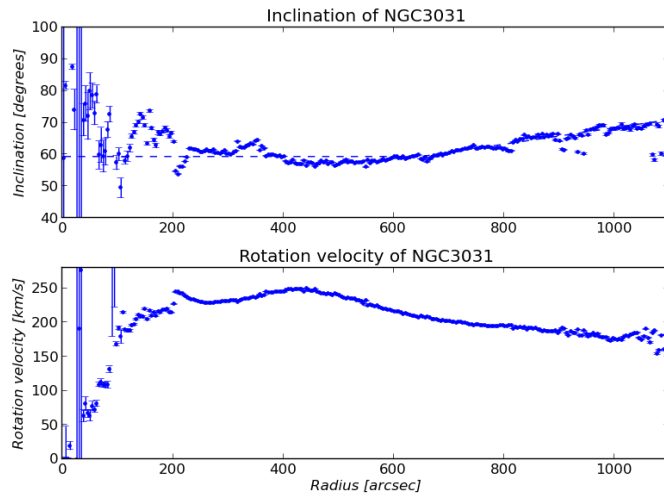


Figure 36: ROTCUR fits the dotted values. The dashed line shows the used curve (model) in the next fitting step. At radii greater than 600 arcsec the modeled line is hard to see, but it matches. Anti-correlation can be seen at 200 arcsec. Where the rotation curve gets a sudden growth, the inclination is fitted with a sudden descent. Inner parts of the galaxy are assumed to have a constant inclination; ROTCUR seems to be less accurate here.

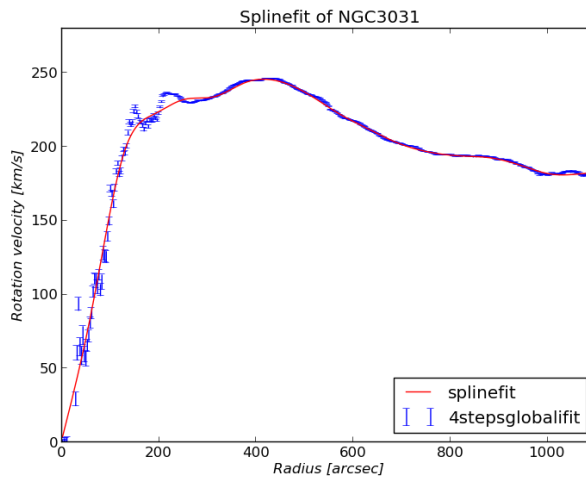


Figure 37: ROTCUR fits the blue values determined while letting the inclination constant at the inner regions. The red line shows the used curve in our modeled velocity field. This spline is fitted by eye: bumps around 200 arcsec are 'removed' by the fit.

11.3 Results

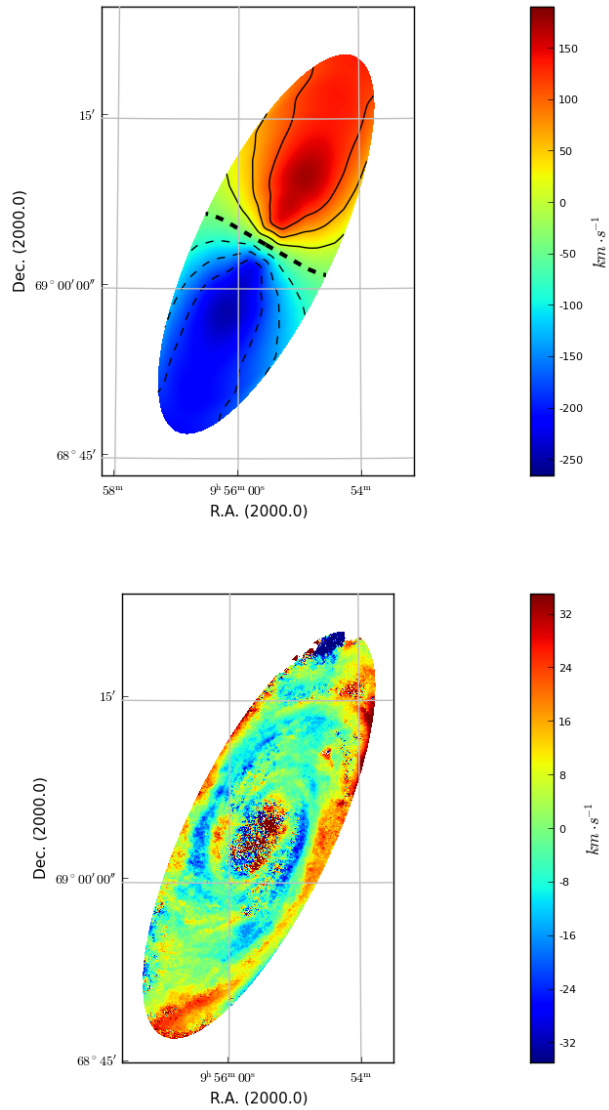


Figure 38: Upper image: Shown is the modeled velocity field created by the program VELFI. All the modeled parameters from the step-by-step procedure are used. Contours are shown spaced by 50 km/s around the systemic velocity of -36 km/s. Lower image: Shown is the observed residual velocity field obtained by subtraction the modeled velocity field from the observed one. On the minor axis streaming motions are clearly visible. These motions seem the follow the spiral structure as confirmed in the next image.

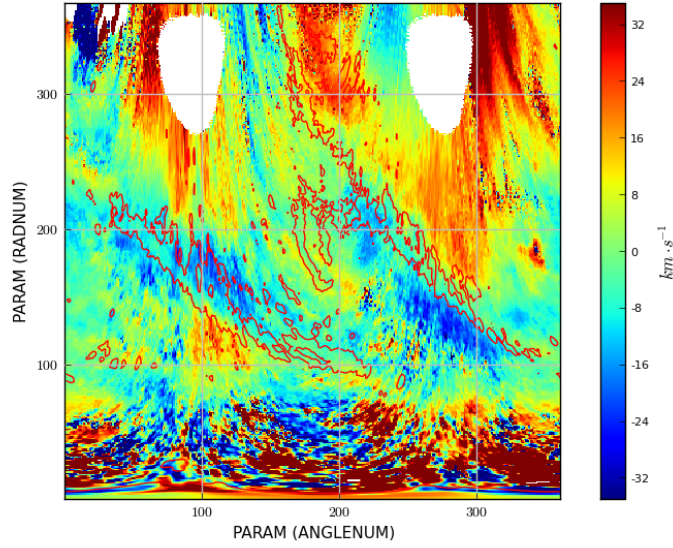


Figure 39: The same observed residual velocity field but now in the galactic coordinates. A contour of the HI image is also shown. It locates the strong presence of the spiral arms. Around the minor axis (90 and 270 degrees) blank data appear. A small error in the calculations probably happened.

12 Appendix C: NGC3621

12.1 Data

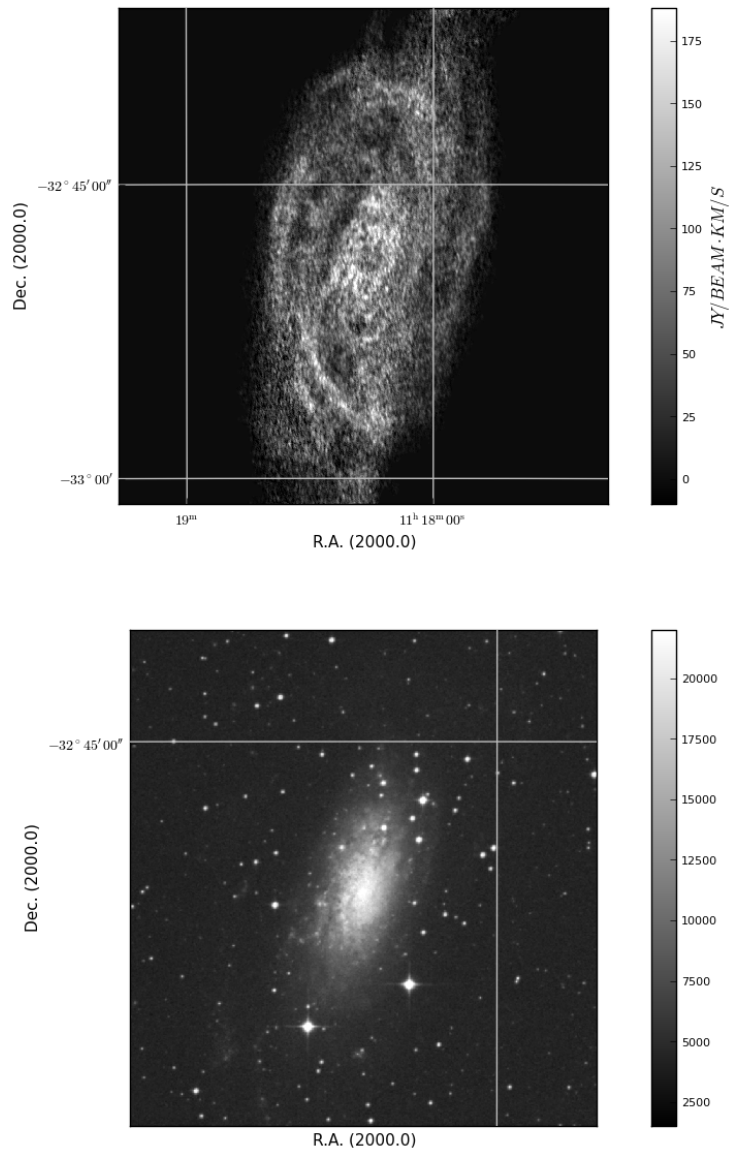


Figure 40: Upper image: Integrated HI map (THINGS). At a distance of roughly 8 arcmin two spiral arms are visible. Lower image: Optical image (r-band) taken from DSS. The structure of the spiral arms is not visible in this image. [15arcmin = 29kpc]

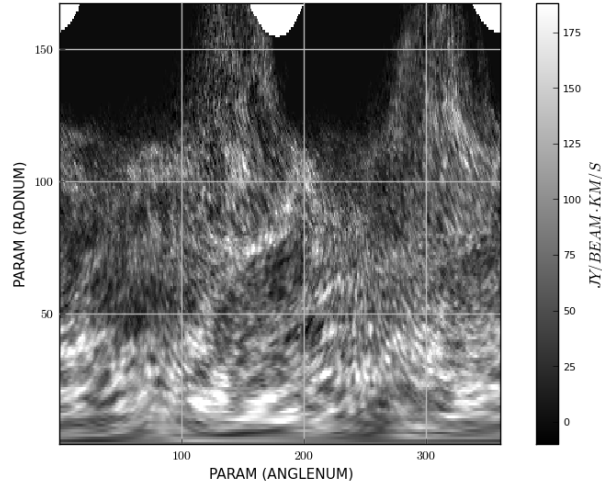


Figure 41: The same integrated HI map, but now in galactic coordinates. On the x-axis the angle θ is shown. It is defined to be angle from the position angle taken in anti-clockwise direction. On the y-axis the radius number is shown. In this image an increase of 1 radnum means an increase of 5 arcseconds in radius. At angle number 200 and radius number 100 the spiral arm can be seen.

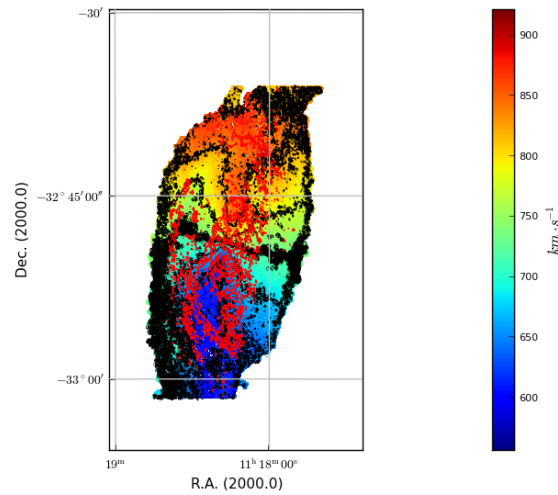


Figure 42: Observed HI velocity field with iso-velocity contours (black) spaced by 50 km/s around the systemic velocity at 729 km/s. A contour of the HI spiral arms is also drawn in red.

12.2 Fitted parameters

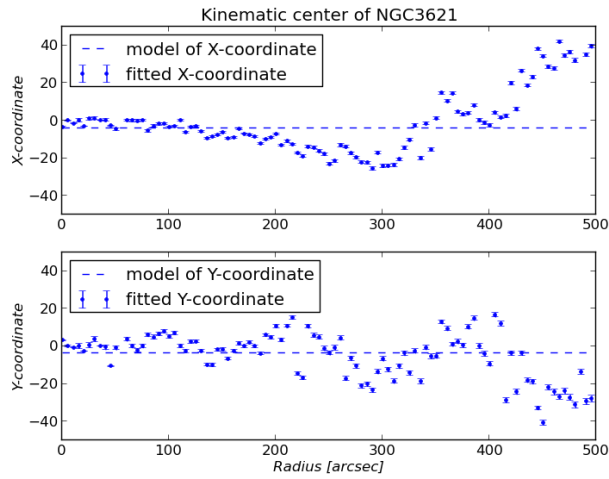


Figure 43: ROTCUR fits the dotted values. The dashed lines show the used values for the kinematic center (model) in the next fitting steps. The determination of the kinematic center is done over the inner part of the HI velocity map.

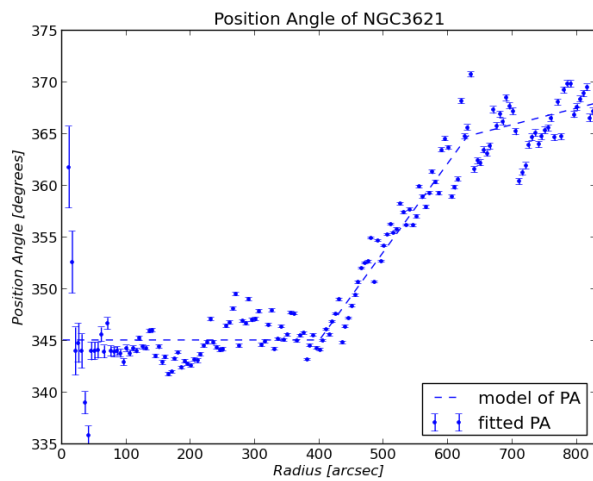


Figure 44: ROTCUR fits the dotted values. The dashed line shows the used curve (model) in the next fitting steps. Upward of 400 arcsec the position angle rapidly rises. This is clearly seen in the modeled velocity field.

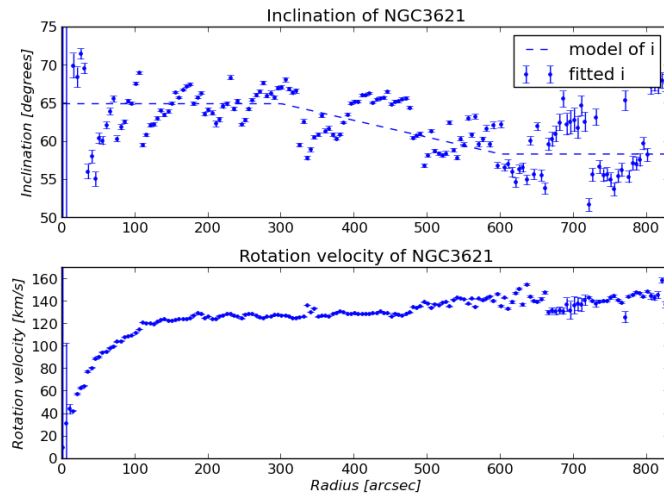


Figure 45: ROTCUR fits the dotted values. The dashed line shows the used curve (model) in the next fitting step. The fitted values are oscillating a lot; our model does not, with the aim of getting rid of irregularities caused by spiral arms.

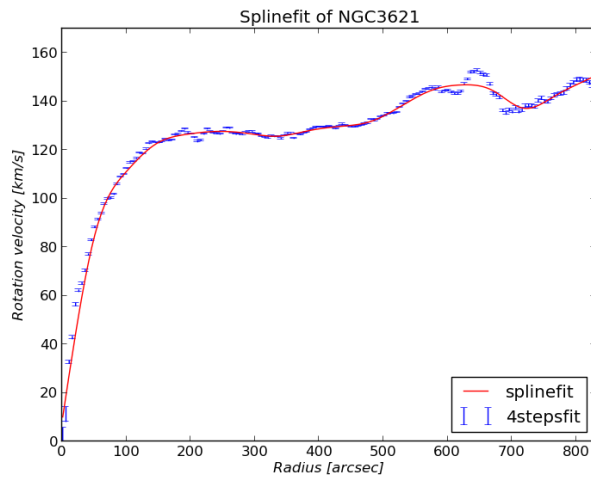


Figure 46: ROTCUR fits the blue values determined while letting the inclination constant at the inner regions. The red line shows the used curve in our modeled velocity field. This spline is fitted by eye: bumps around 200 arcsec are 'removed' by the fit. A strange bump can be seen around 600 arcsec.

12.3 Results

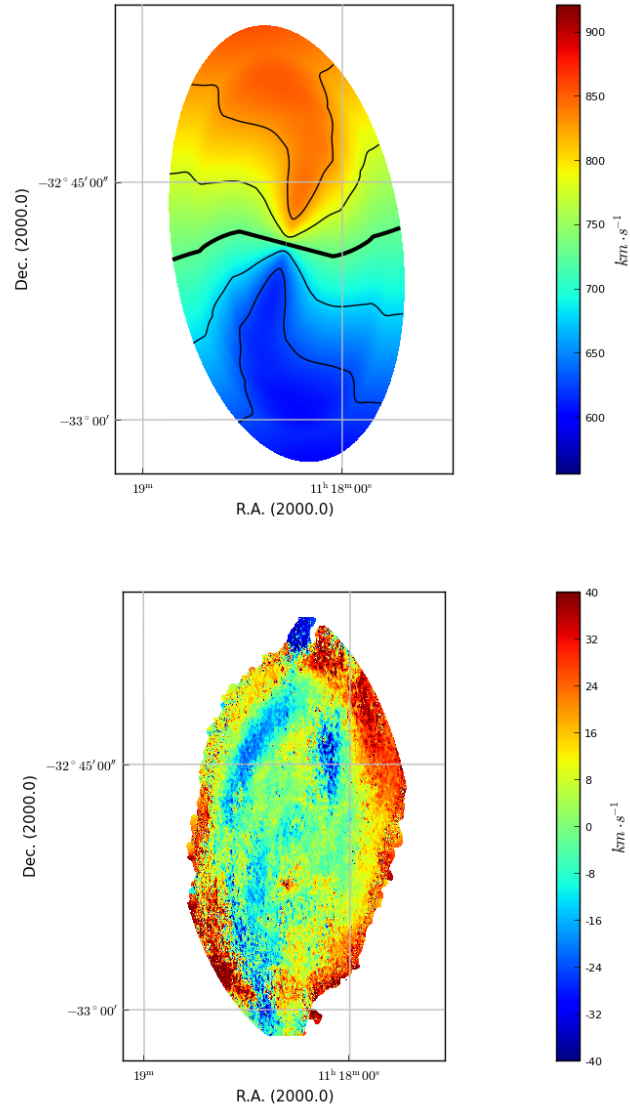


Figure 47: Upper image: Shown is the modeled velocity field created by the program VELFI. All the modeled parameters from the step-by-step procedure are used. Contours are shown spaced by 50 km/s around the systemic velocity of 729 km/s. Lower image: Shown is the observed residual velocity field obtained by subtraction the modeled velocity field from the observed one. On the upper part of the image streaming motions are clearly visible. However, the HI integrated image does not show a dominant spiral structure in the upper left part.

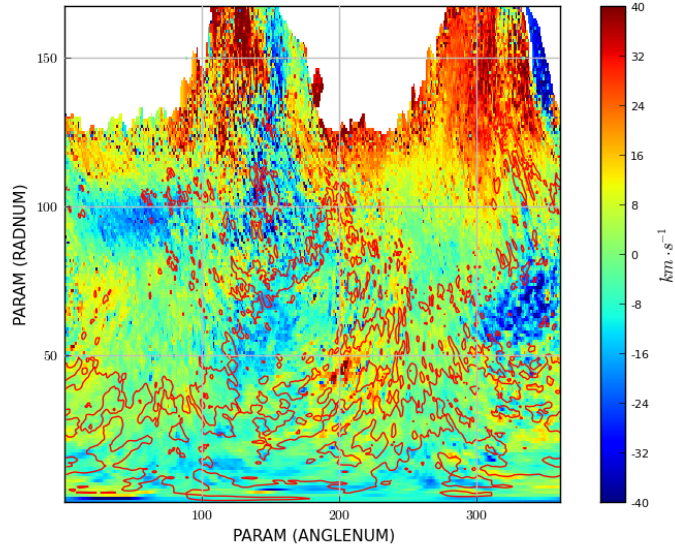


Figure 48: The same observed residual velocity field but now in the galactic coordinates. A contour of the HI image is also shown. The red area at the upper right part of the image attracts attention. At these radii the model is not good anymore. This can be seen by comparing the model with the observed velocity field. The observed velocities of this galaxy do not seem to be symmetric. The bump in the rotation curve may also be wrong. We conclude that the model seems good at radii with $r < 450$ arcsec. At larger radii the fitted position angle rapidly rises. In addition the kinematic center starts to deviate from the modeled center at these same radii.

13 Appendix D: NGC5194 (M51)

13.1 Data

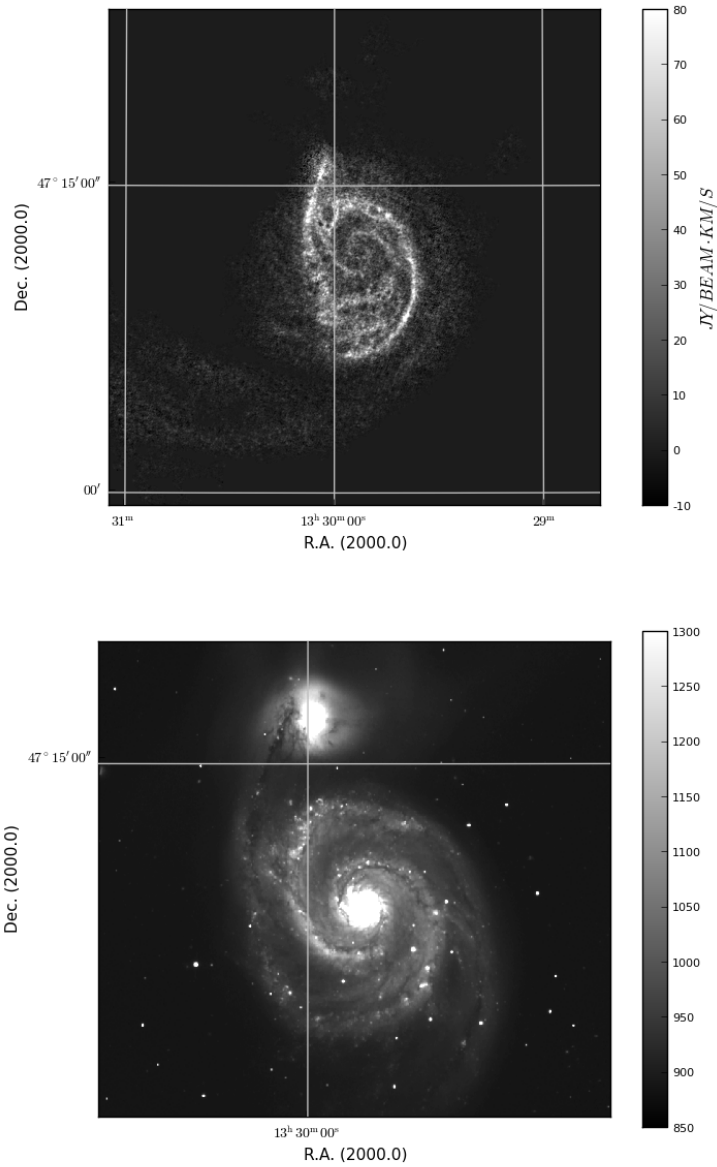


Figure 49: Upper image: Integrated HI map (THINGS). In this galaxy the two HI spiral arms can be seen very well. Lower image: Optical image (r-band) taken from SDSS. The outer part of the spiral arms are better visible in the HI image, the inner parts better in the r-band image. [$15arcmin = 35kpc$]

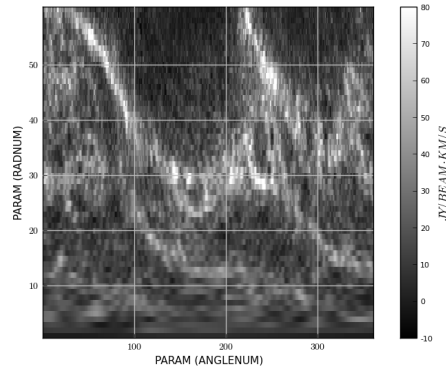


Figure 50: The same integrated HI map, but now in galactic coordinates. On the x-axis the angle θ is shown. It is defined to be angle from the position angle taken in anti-clockwise direction. On the y-axis the radius number is shown. In this image an increase of 1 radnum means an increase of 5 arcseconds in radius, so this map shows the inner part of the galaxy up to a distance of 300 arcsec (12 kpc). Nevertheless, only the very outer parts of the galaxy are not shown in this map. At those large radii tidal interactions disturb the rotation curve of the galaxy.

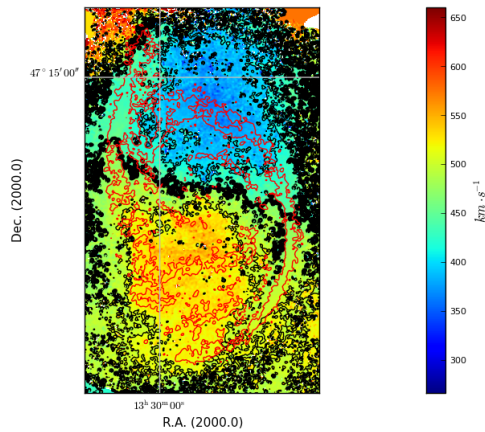


Figure 51: Observed HI velocity field with three iso-velocity contours (black) spaced by 50 km/s around the systemic velocity at 459 km/s. A contour of the HI spiral arms is also drawn in red, which shows that almost the entire HI spiral arms lie within the regime where tidal interactions do not play such a great role yet. On the edges of the image you see that they do. On the upper part the approaching side suddenly changes to receding side and vice versa as seen on the lower left side of the image.

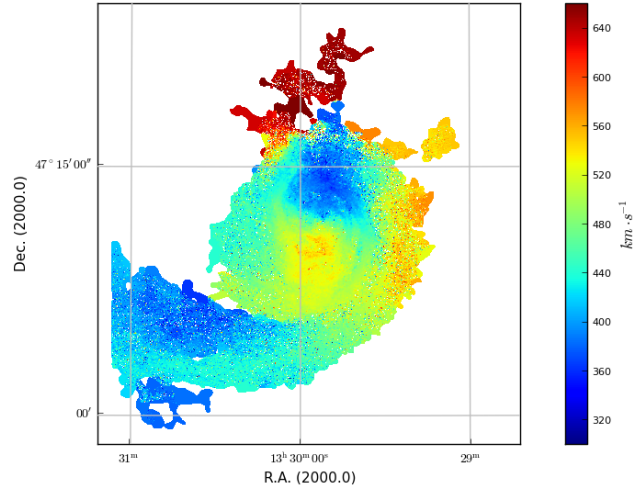


Figure 52: The entire observed HI velocity field. There is not one receding or approaching side, indicating that the interaction with M51b is not negligible. The position angle changes dramatically with increasing radius. In the outer regions to little data is available to say something about the position angle.

13.2 Fitted parameters

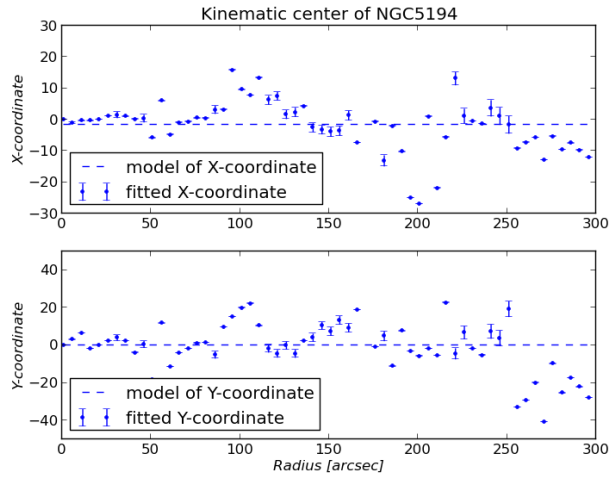


Figure 53: ROTCUR fits the dotted values. The dashed lines show the used values for the kinematic center (model) in the next fitting steps. Only the inner part of the galaxy is used (up to 300 arcsec). At radii larger than 250 arcsec the kinematic center slightly starts to decrease in both x- and y-coordinate and the model may be less accurate.

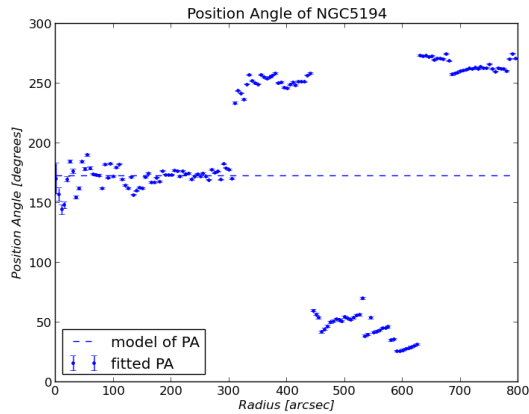


Figure 54: ROTCUR fits the dotted values. The dashed line shows the used curve (model) in the next fitting steps. Note that the model does not match the fitted values anymore at radii larger than 300 arcsec. That is fine since we will not use these values: at those radii from the kinematic center, the interactions with M51b starts to play a role in the dynamics of the gas flow. The observed velocity field already gave away the shape of the position angle.

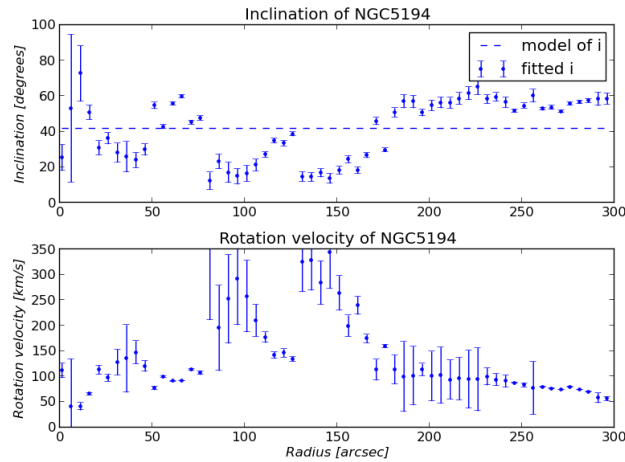


Figure 55: ROTCUR fits the dotted values. The dashed line shows the used curve (model) in the next fitting steps. Anti-correlation can be seen over the entire graph. Where the rotational velocity grows, the fitted inclination goes down. The inclination of the galaxy is assumed to be constant, at least in the region within 300 arcsec. A weighted average is taken to calculate the inclination for the model.

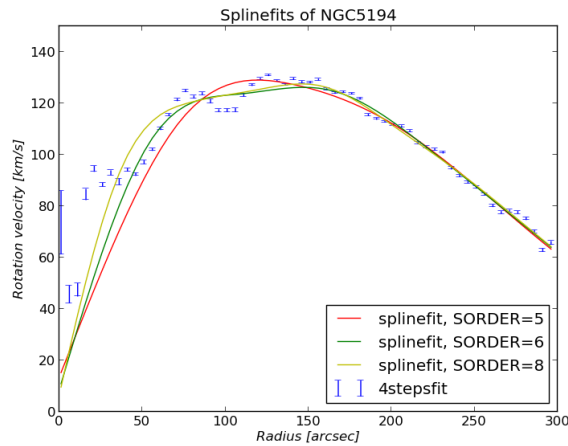


Figure 56: ROTCUR fits the blue values determined while letting the inclination constant. The colored lines show three different splines. The yellow spline with SORDER=8 is chosen to use in our model velocity field, since it carries velocities which fit the results of ROTCUR the best in the inner region with radius less than 100 arcsec, although the red line has a much more smooth shape. At radii larger than 150 arcsec all splines are roughly equal. Bumps between 50 and 150 arcsec are 'removed' by the fit.

13.3 Results

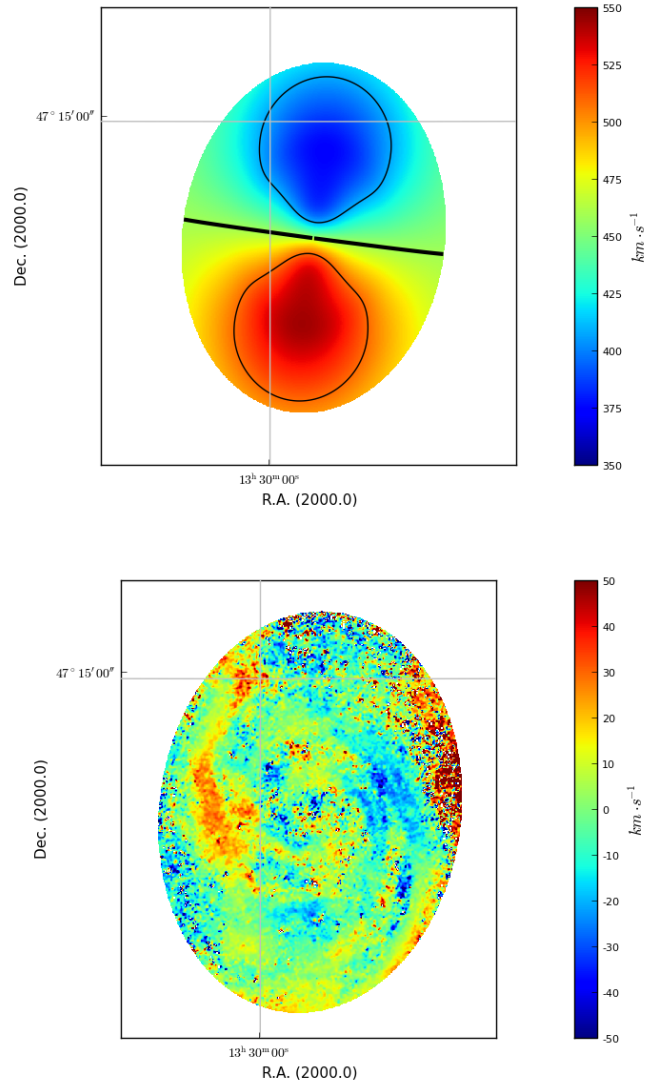


Figure 57: Upper image: Shown is the modeled velocity field created by the program VELFI. All the modeled parameters from the step-by-step procedure are used. Contours are shown spaced by 50 km/s around the systemic velocity of 459 km/s. At $r > 250$ arcsec the model is less good, since the assumption of symmetry seems not to be correct when taking a look at the observed velocity field. Lower image: Shown is the observed residual velocity field obtained by subtraction of the modeled velocity field from the observed one. The streaming motions are not as clear as the ones in NGC3031, although it was expected since the spiral arms are very dominant.

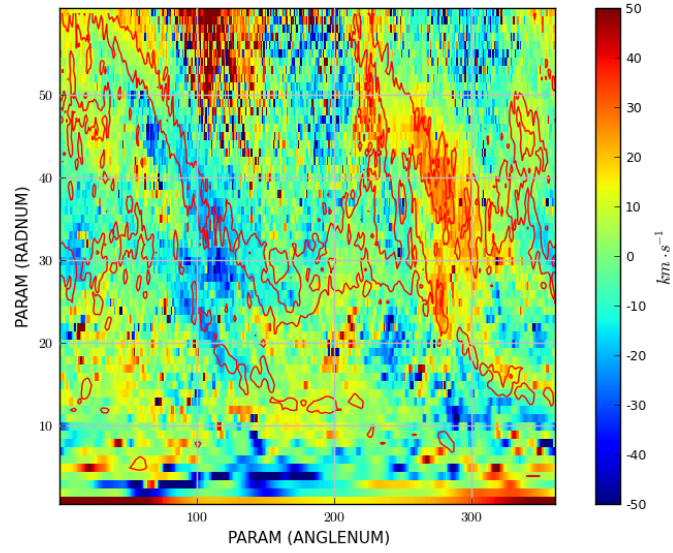


Figure 58: The same observed residual velocity field but now in the galactic coordinates. A contour of the HI image is also shown. It is hard to see any relation between residual velocities and the location of the spiral arms. Note that this might be caused by the stretching effect of ELLPROF along the minor axis.

14 Appendix E: NGC6946

14.1 Data

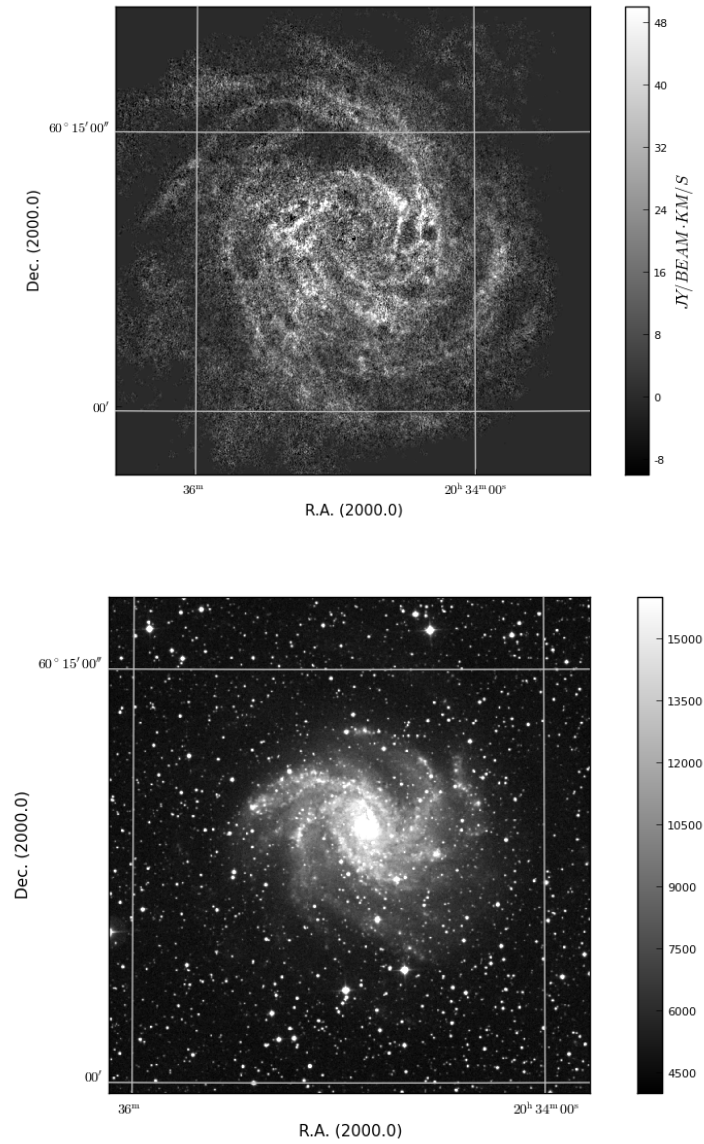


Figure 59: Upper image: Integrated HI map (THINGS). Spiral structures are visible but it is difficult to identify a tight shape and specific location of a spiral arm, because it seems to consist of lots of tiny subarms. Lower image: Optical image (r-band) taken from DSS. The structure of the innermost spiral arms are better visible in this image. [$15 \text{ arcmin} = 25 \text{ kpc}$]

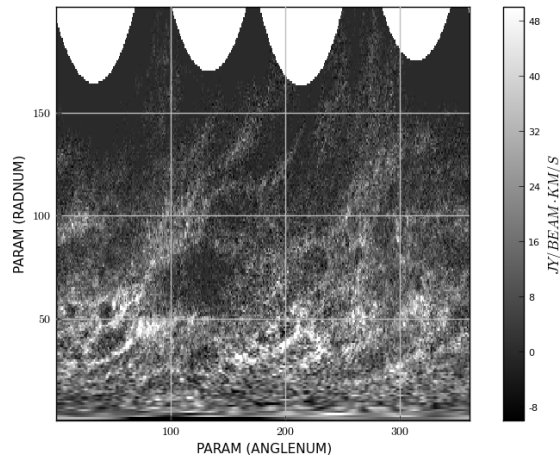


Figure 60: The same integrated HI map, but now in galactic coordinates. On the x-axis the angle θ is shown. It is defined to be angle from the position angle taken in anti-clockwise direction. On the y-axis the radius number is shown. In this image an increase of 1 radnum means an increase of 5 arcseconds in radius. The weak spiral structure is better visible in this type of view.

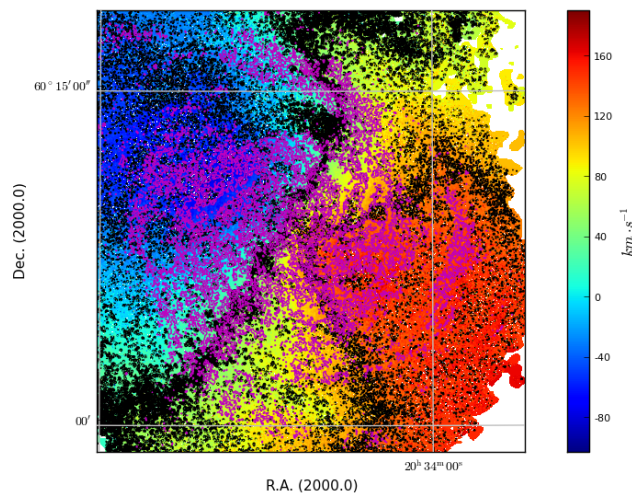


Figure 61: Observed HI velocity field with three iso-velocity contours (black) spaced by 80 km/s around the systemic velocity at 42 km/s. A contour of the HI spiral arms is also drawn in magenta.

14.2 Fitted parameters

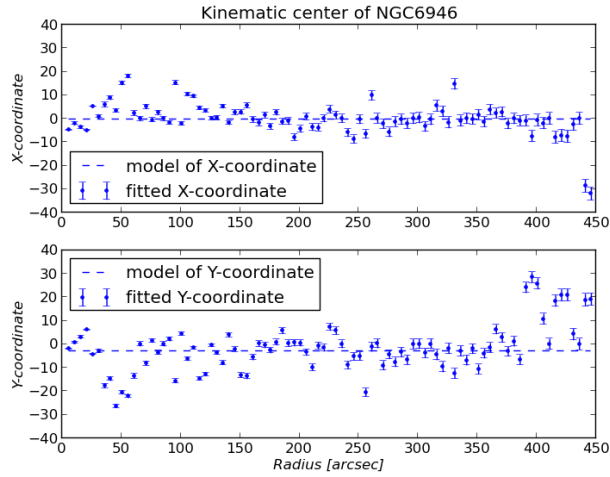


Figure 62: ROTCUR fits the dotted values. The dashed lines show the used values for the kinematic center (model) in the next fitting steps.

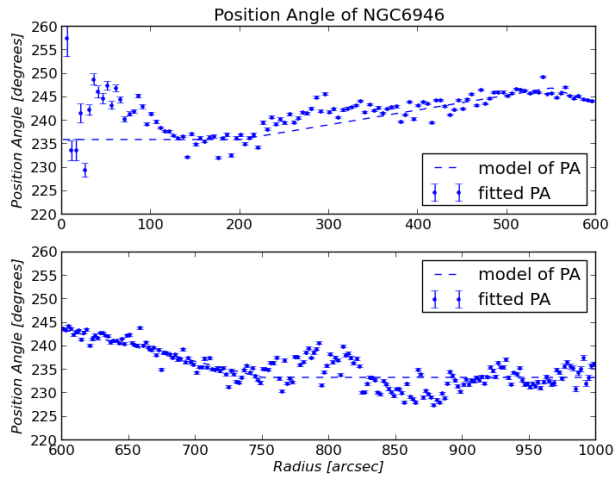


Figure 63: ROTCUR fits the dotted values. The dashed line shows the used curve (model) in the next fitting steps. Note that the model again assumes a constant position angle at the center. The bumps and dips around 825 arcsec can be caused by the two outermost HI spiral arms (not visible in the DSS image).

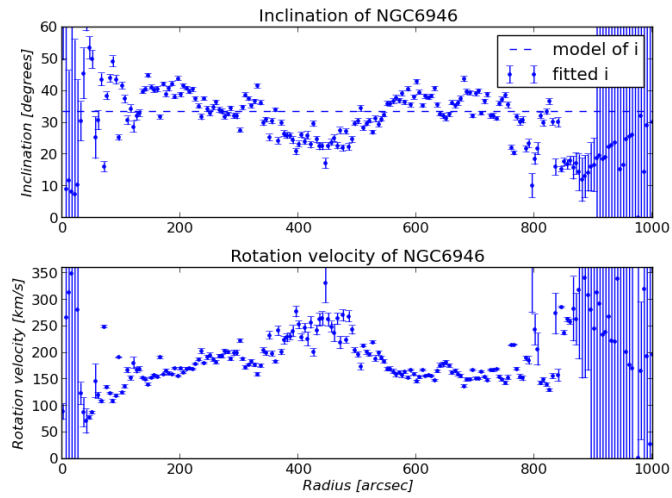


Figure 64: ROTCUR fits the dotted values. The dashed line shows the used curve (model) in the next fitting steps. Anti-correlation can be seen in the entire graph. The galaxy is assumed to have a constant inclination. Note that ROTCUR has problems with fitting in the innermost regions and outermost regions. Therefore it is better not to use the results with radii larger than 800 arcsec and smaller than 100 arcsec.

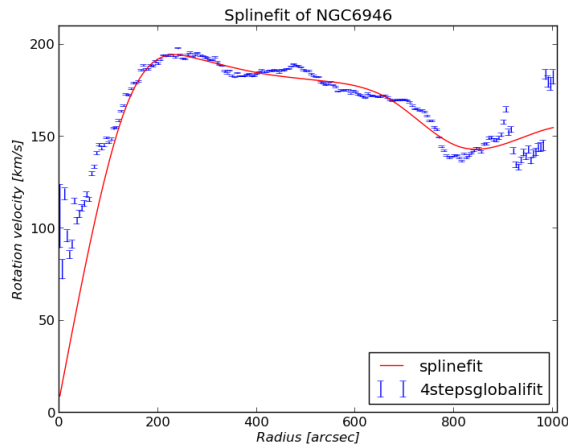


Figure 65: ROTCUR fits the dotted blue values determined while letting the inclination constant. The red line shows the used curve in our modeled velocity field. This spline is fitted by eye: the region between 300 and 700 arcsec is smoothed by the fit. At radii larger than 700 arcsec we do not attach importance to the spline anymore since the fitted results are not reliable there.

14.3 Results

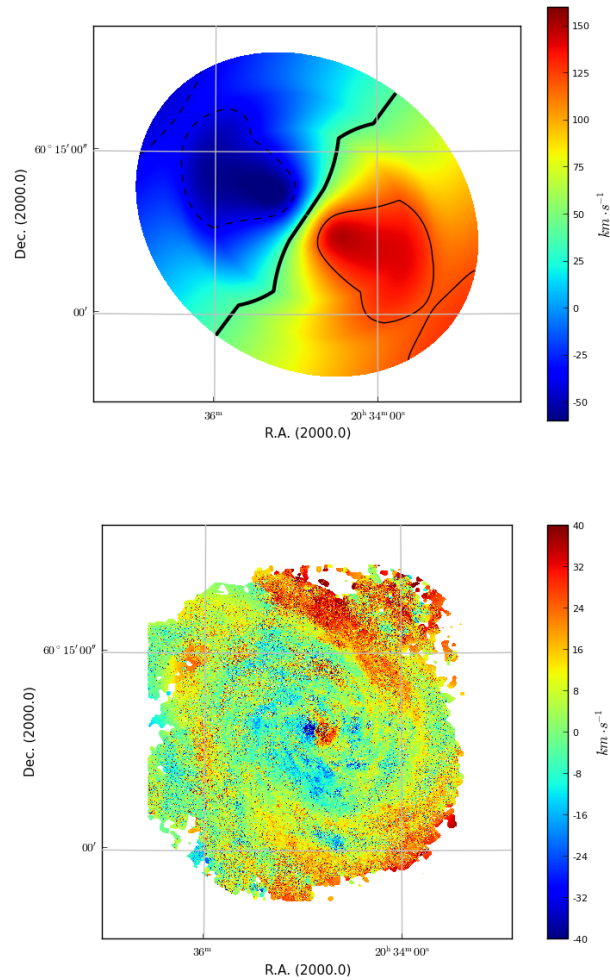


Figure 66: Upper image: Shown is the modeled velocity field created by the program VELFI. All the modeled parameters from the step-by-step procedure are used. Contours are shown spaced by 80 km/s around the systemic velocity of 42 km/s. Note that the upper part and lower right part (near the major axis) of the model do not match the observed HI velocities anymore at radii larger than 700 arcsec, whereas the lower left part does. The galaxy is not symmetric at those radii. Lower image: Shown is the observed residual velocity field obtained by subtraction the modeled velocity field from the observed one. The structure we see does not reveal lots of streaming motions. The center of the image shows a little ellipse where one might appoint a receding and approaching side. The model should have removed this: the model is not correct in the center. The large positive residues on top and on the lower right part of the field are due to the fact that the model is not correct there.

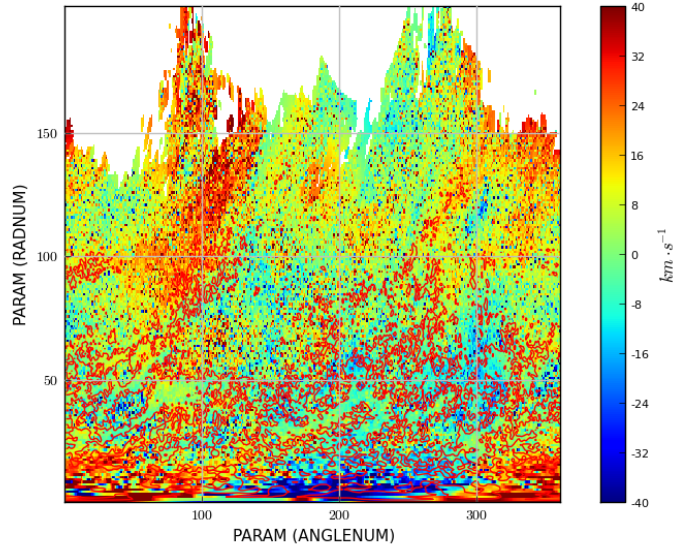


Figure 67: The same observed residual velocity field but now in the galactic coordinates. A contour of the HI image is also shown. Unfortunately we do not see clear streaming motions in the correct modeled part of this galaxy.